Determination of 3D Flame Surface Density variables from 2D measurements: Validation using Direct Numerical Simulation

Nilanjan Chakraborty [a)*], Evatt R. Hawkes[b)]

a) Engineering Department, Liverpool University, Brownlow Hill, Liverpool, L69 3GH, U.K.

b) School of Photovoltaic and Renewable Energy Engineering/School of Mechanical and Manufacturing Engineering, The University of New South Wales, Sydney, NSW 2052, Australia

E-mail address: n.chakraborty@liverpool.ac.uk
Phone No: +44 0151 794 4831
Fax No: +44 0151 794 4848

(Received

* Corresponding author

ABSTRACT

Three-dimensional compressible Direct Numerical Simulation (DNS) data of freely propagating statistically planar turbulent premixed flames has been used to assess the accuracy of the isotropy derived correction factors, which relate the two-dimensional projections of the different terms of the Reynolds averaged flame-surface density (FSD) transport equation with their corresponding actual three-dimensional counterparts for different values of Karlovitz number Ka, Lewis number Le, heat release parameter τ, and turbulent Reynolds number Re_t. It is shown that the isotropic distribution of the surface area weighted probability density function (pdf) of the angle ϕ between the normal vectors on the measurement plane and on the flame surface provides a simple algebraic relation between the generalised FSDs evaluated in two and three dimensions (i.e. Σ_{2D} and Σ_{3D}), irrespective of the values of Ka, τ, Le and Re_t. Isotropic relations between two-dimensional and three-dimensional counterparts of the surface-averaged curvature and the FSD propagation term are also found to work well for all the values of Ka, τ, Le and Re_t considered in this study. However, the relations between the value obtained from two-dimensional projection and the actual three-dimensional value for the tangential strain rate and curvature terms in the FSD transport equation work well only for the high values of turbulent Reynolds number. The reasons behind the disagreement between the predictions of the relations derived based on isotropy arguments for both the tangential strain rate and curvature terms of the FSD transport equation are explained in detail. It is found that the threshold value of Re_t above which the assumption of isotropy yields an accurate relation between two-dimensional projection and three-dimensional values for the tangential strain rate and curvature terms of the FSD transport equation depends on the values of heat release parameter, Lewis number and the regime of the prevailing combustion process.

I. INTRODUCTION

The Flame Surface Density (FSD) based reaction rate closure is one of the most popular approaches in turbulent premixed combustion modelling. This methodology is well-established in the context of Reynolds Averaged Navier Stokes (RANS) modelling[1-3] and in recent times this closure technique has been extended for Large Eddy Simulations (LES) of turbulent premixed flames.[4-11] The statistics of FSD and the various terms of its transport equation have been extensively studied using Direct Numerical Simulations (DNS)[4,9-14] and experimental measurements.[15-29] There have been many studies on experimental measurements of FSD and a detailed discussion is provided in the review paper by Driscoll.[17] In most experimental measurements, the flame location and structure are identified by Rayleigh scattering, Planar Laser Induced Fluorescence (PLIF) and tomography of small vaporising droplets, while the velocity and velocity gradient measurements are carried out using Particle Image Velocimetry (PIV). Very often these measurements have been carried out in two-dimensions for the measurements of FSD[15-29], curvature [15,16,21-23,26-28,31-36], strain rate[19,21,37] and curvature-stretch rate[30] (with displacement speed assumed to be equal to laminar burning velocity[15,16,20,23,37]). As these measurements cannot capture the three-dimensional flame propagation and the species and velocity fields associated with it, corrections are warranted for obtaining true three-dimensional values from two-dimensional measurements. The only three-dimensional measurements of all of the relevant quantities were obtained in studies of liquid autocatalytic reaction fronts.[38] Recently, a few three-dimensional measurements[19,33,39] have been carried out where the experimental data is obtained from the intersection line of two intersecting planes. Such methods are still very expensive and thus two-dimensional measurements will have relevance in the foreseeable future. This fact essentially necessitates the estimatation of the correction factors for two-dimensional measurements so that experimental data can be used for developing new models and assessing

the performance of new models. Recently, Hawkes *et al.*[40] proposed correction factors for two-dimensional measurements of FSD and the various terms of the FSD transport equation based on assumed isotropy of the angle between the normal vectors on the measurement plane and the local flame surface, and other simplifications which arose from isotropic assumptions. Hawkes *et al.*[40] compared corrected two-dimensional Reynolds averaged data with the corresponding actual three-dimensional Reynolds averaged quantities using a detailed chemistry based three-dimensional DNS data of slot-jet Bunsen flame configuration[40,41] and good agreement was obtained. However, because of the large simulation cost of those simulations, only a limited parametric range was studied, and so the validity of the assumption related to isotropy in relation to turbulent Reynolds number Re_t and global Lewis number $Le = \alpha_T / D$ is yet to be assessed (where α_T and D are the thermal diffusivity and mass diffusivity respectively). In the present study, the above issues are assessed using a three-dimensional compressible DNS database with simplified chemistry with reasonable variations of heat release parameter, $\tau = (T_{ad} - T_0)/T_0$, Re_t and Le, where T_{ad} and T_0 are the adiabatic flame temperature and unburned gas temperature respectively. In real combustion situations it is difficult to assign a single Lewis number to characterise the whole combustion process but in several previous analytical[42,43] and DNS[12,44-48] studies a global Lewis number was used to study the effects of differential molecular transport of heat and mass in isolation and the same procedure has been followed here. Moreover, the effects of flame normal acceleration are typically relatively strong in flames within the corrugated flamelets regime[49] where the flame thickness is smaller than the Kolmogorov length scale. As a result of this, strong flame normal acceleration may induce strong directionality and the assumption of isotropy may be rendered invalid. On the other hand, in the thin reaction-zones regime combustion,[49] the effects of flame-normal acceleration can be

partially masked by turbulent processes as energetic turbulent eddies penetrate into the preheat zone due to the flame being thicker than the Kolmogrov length scale, so the assumption of isotropy may work satisfactorily in the flames belonging to the thin reaction zones regime combustion, or indeed in regimes of even higher *Ka*. In this respect the main objectives of the present study are as follows:

1. To assess the predictive capabilities of the relations derived by Hawkes *et al.*[40] for obtaining three-dimensional quantities related to the FSD transport from two-dimensional measurements for flames with comparable turbulent Reynolds number representing the corrugated flamelets and thin reaction zones regimes of turbulent premixed combustion.
2. To assess the validity of the assumptions related to isotropy made by Hawkes *et al.*[40] in response to the variations of heat release parameter τ, turbulent Reynolds number Re_t and global Lewis number Le.

The rest of the paper is organised as follows. The necessary mathematical background will be provided in the next section of this paper. This will be followed by a brief description of numerical implementation. Following this, results will be presented and subsequently discussed. Finally the main findings will be summarised and conclusions will be drawn.

II. MATHEMATICAL BACKGROUD

Ideally combustion DNS studies should be carried out in three-dimensions with detailed chemistry. Until recently most combustion DNS studies have been carried out either in two-dimensions with detailed chemistry or in three-dimensions with simplified chemistry due to the limitation of computational effort and data storage capacity. Although advances in computational

capacity have recently enabled three-dimensional detailed chemistry based DNS, they still remain very expensive (millions of computational hours per run as indicated by Chen *et al.* [50]), and therefore prohibitive for extensive parametric variations as carried out in this paper. For the present paper, simplified chemistry based three-dimensional compressible DNS databases have been considered where the reaction mechanism is accounted for by a single step Arrhenius-type chemical reaction. In the context of simplified chemistry, a reaction progress variable c can be defined in terms of the reaction mass fraction Y_R so that it increases monotonically from zero in unburned gases to unity in fully burned products.

Relations between the two-dimensional measured values and three-dimensional reality will now be presented following Hawkes *et al.*[40] Various assumptions will be invoked while deriving these relations. Isotropy of the scalar and flow fields provides a sufficient condition to meet these assumptions, but it is not a necessary one, and some of the relationships are more general than complete isotropy. It is further assumed here that the measurement plane contains the basic geometry of the mean flow field, and that the out-of plane direction is statistically homogeneous, i.e. there are no gradients of mean quantities in that direction – e.g. a vertical slice through the middle of a jet flame.

The geometrical framework behind the relations between the three-dimensional quantities and their two-dimensional counterparts

The actual generalised FSD in three-dimensions Σ_{gen} is defined in the following manner (Ref. 4):

$$\Sigma_{gen} = \Sigma_{3D} = \overline{\Sigma_3} = \overline{|\nabla c|} \ , \qquad (1)$$

where $\Sigma_3 = |\nabla c|$ is a generalised fine-grained surface density function, and the overbar signifies a Reynolds averaging operation. In this paper Σ_{gen} represents the actual FSD in three-dimensions (i.e. $\Sigma_{3D} = \Sigma_{gen} = \overline{\Sigma_3}$). The transport equation of the generalised FSD is given by (Ref. 51):

$$\frac{\partial \Sigma_{gen}}{\partial t} + \frac{\partial \overline{(u_j)_s \Sigma_{gen}}}{\partial x_j} = \overline{(a_T)} \Sigma_{gen} + 2\overline{(S_d \kappa_m)_s \Sigma_{gen}} - \frac{\partial \overline{(S_d N_i)_s \Sigma_{gen}}}{\partial x_i}, \quad (2)$$

where $a_T = (\delta_{ij} - N_i N_j) \partial u_i / \partial x_j$ is the tangential strain rate, $N_i = -\partial c / \partial x_i / |\nabla c|$ and u_i are the i^{th} component of flame normal and velocity vectors respectively, $S_d = (Dc/Dt)/|\nabla c|$ is the displacement speed, $\kappa_m = \nabla . \vec{N} / 2 = (\kappa_1 + \kappa_2)/2$ is the local flame curvature with κ_1 and κ_2 being the principal curvatures of the flame surface and $\overline{(Q)}_s = \overline{Q|\nabla c|} / \overline{|\nabla c|}$ is the surface averaged value of a general variable Q.[1-4,9-16] The physical significances of the various terms of the FSD transport equation are as follows. The two terms on left hand side on eq. 2 signify the effects of unsteadiness and mean advection whereas the first two terms on the right hand side denote the contributions of stretch rate induced by tangential strain rate and curvature respectively. The last term on right hand side arises due to propagation of premixed flames in the flame normal direction. The terms on the right hand side of eq. 2 are commonly referred to as the tangential strain rate, curvature and propagation terms, respectively.[9-16] In the subsequent discussion, the relations between two-dimensional measurements of these quantities and their actual three-dimensional values will be considered. In order to do so, Fig. 1 will be considered, where the copper coloured surface in Fig. 1a represents the flame surface whereas the measurement plane and tangent plane passing through point P are shown in blue and grey colours respectively. The angles and co-ordinate systems which will be used for the following analysis are shown in Fig.

1b without the obstruction due to the flame surface. The laboratory co-ordinate is shown by the orthogonal system $\vec{b}$ where $b_1 - b_2$ plane represents the measurement plane and the out of plane direction is given by b_3. In Fig. 1b, distances along b_1 and b_2 axes are shown by y_{b_1} and y_{b_2} respectively. The measured two-dimensional FSD is given by:

$$\Sigma_{2D} = \overline{\Sigma_2} = \overline{\sqrt{\left(\frac{\partial c}{\partial y_{b_1}}\right)^2 + \left(\frac{\partial c}{\partial y_{b_2}}\right)^2}} \quad . \tag{3a}$$

where Σ_2 is given by:

$$\Sigma_2 = \sqrt{\left(\frac{\partial c}{\partial y_{b_1}}\right)^2 + \left(\frac{\partial c}{\partial y_{b_2}}\right)^2} \quad . \tag{3b}$$

The quantities Σ_2 and Σ_3 are related by:

$$\Sigma_2 = \Sigma_3 \cos\phi \ , \tag{3c}$$

where ϕ is the angle between the measurement plane and flame normal vector. The surface averaging operation in two-dimensions is given by:

$$\overline{(Q)}_{s2} = \overline{Q\Sigma_2} / \Sigma_{2D} \ . \tag{3d}$$

Using eqs. 3c and d one obtains:

$$\Sigma_{2D} = \Sigma_{3D} \overline{(\cos\phi)}_s = \Sigma_{gen} \overline{(\cos\phi)}_s \tag{3e}$$

The above correction of two-dimensional FSD also applies to the temporal rate of change term and to the mean convective terms of the FSD transport equation if the out of plane convection is neglected (which is usually possible in the typical experimental situations such as jet flames, expanding spherical flames, rod-stabilised V-flames, etc).[40] An isotropic distribution of ϕ is

obtained if the probability of finding an angle ϕ within the differential change of angle $d\phi$ is assumed to be proportional to the area swept on the unit ball defining all possible orientations of flame normal vector $\vec{N}$. Under this situation the surface area weighted probability density function (pdf) of ϕ can be assumed as (Ref. 40):

$$P(\phi) = \cos\phi / 2 \ , \tag{3f}$$

which yields:

$$\overline{(\cos\phi)}_s = \frac{1}{2}\int_{-\pi/2}^{\pi/2} \cos^2\phi \, d\phi = \frac{\pi}{4} \ . \tag{3g}$$

Equation 3g can be used in eq. 3e to yield:

$$\Sigma_{gen} = \Sigma_{3D} = \Sigma_{2D}(4/\pi) \tag{4}$$

The unit vectors in the tangential directions $\vec{t}_1$ and $\vec{t}_2$ according to orthogonal system in Fig. 1 can be defined as:

$$\vec{t}_1 = \frac{\vec{N} \times \vec{b}_3}{\left|\vec{N} \times \vec{b}_3\right|} \quad ; \quad \vec{t}_2 = \vec{N} \times \vec{t}_1 \ . \tag{5}$$

The unit vector $\vec{t}_1$ runs along the intersection of tangent and measurement planes.

Relation between the three-dimensional tangential strain rate term and its two-dimensional projection

According to eq. 5 the tangential strain rates in three and two dimensions (i.e. a_T and a_{T2D}) are given by:

$$a_T = \left(\frac{\partial u_{t_1}}{\partial x_{t_2}} + \frac{\partial u_{t_2}}{\partial x_{t_1}} \right) \text{ and } a_{T2D} = \frac{\partial u_{t_1}}{\partial x_{t_2}} \ , \tag{6a}$$

where u_{t_1} and u_{t_2} are velocity components along in the tangential directions $\vec{t}_1$ and $\vec{t}_2$ respectively and x_{t_1} and x_{t_2} are the coordinates in the tangential directions $\vec{t}_1$ and $\vec{t}_2$ respectively. This gives rise to:

$$\overline{a_T \cos\phi \Sigma_3} = \overline{\left(\frac{\partial u_{t_1}}{\partial x_{t_2}} + \frac{\partial u_{t_2}}{\partial x_{t_1}}\right)\Sigma_2} = \overline{\left(\frac{\partial u_{t_1}}{\partial x_{t_2}} + \frac{\partial u_{t_2}}{\partial x_{t_1}}\right)}_{s2} \Sigma_{2D} \ . \qquad (6b)$$

If $\partial u_{t_1} / \partial x_{t_2}$ and $\partial u_{t_2} / \partial x_{t_1}$ are considered to be statistically identical and ϕ is considered to be statistically independent of other variables (isotropy of the flow and scalar fields is a sufficient but not necessary condition for these assumptions), one obtains:

$$\overline{a_T \cos\phi \Sigma_3} = \overline{(a_T)}_s \overline{(\cos\phi)}_s \Sigma_{gen} = \overline{\left(\frac{\partial u_{t_1}}{\partial x_{t_2}} + \frac{\partial u_{t_2}}{\partial x_{t_1}}\right)}_{s2} \Sigma_{2D} = 2\overline{(a_{T2D})}_{s2} \Sigma_{2D} \ . \qquad (6c)$$

This gives rise to:

$$\overline{(a_T)}_s \Sigma_{gen} = \frac{8}{\pi} \overline{(a_{T2D})}_{s2} \Sigma_{2D} \ . \qquad (6d)$$

Relation between the three-dimensional propagation term and its two-dimensional projection

It is assumed here that two-dimensional measurement of displacement speed is estimated based on simultaneous PLIF and PIV measurement so that flame movement can be separated from background fluid movement. Moreover, if the out of plane velocity is negligible or if the two-dimensional displacement speed statistics are conditioned upon negligible out-of-plane fluid velocity, the observed two-dimensional displacement speed S_{d2D} can be expressed as:

$$S_{d2D} = S_d / \cos\phi \ . \qquad (6e)$$

This essentially suggests that:

$$\overline{(S_{d2D})_{s2}}\Sigma_{2D} = \overline{S_{d2D}\Sigma_2} = \overline{\frac{S_d}{\cos\phi}\Sigma_3\cos\phi} = \overline{S_d\Sigma_3} = \overline{(S_d)}_s\Sigma_{gen} \ . \tag{6f}$$

Similarly one can write:

$$\overline{(\rho S_{d2D})_{s2}}\Sigma_{2D} = \overline{\rho S_{d2D}\Sigma_2} = \overline{\frac{\rho S_d}{\cos\phi}\Sigma_3\cos\phi} = \overline{\rho S_d\Sigma_3} = \overline{(\rho S_d)}_s\Sigma_{gen} \ . \tag{6g}$$

The relations given by eqs. 6f and 6g are exact relations and are independent of the assumption of isotropy.

Using the above relations, the quantity $\overline{(S_d N_i)}_s\Sigma_{gen}$ can be written in the following manner if S_d and N_i are assumed to be uncorrelated following the DNS-based evidence (Ref. 9):

$$\begin{aligned}\overline{(S_d N_i)}_s\Sigma_{gen} &= \overline{(S_d)}_s\overline{(N_i)}_s\Sigma_{gen} = -\overline{(S_d)}_s\partial\bar{c}/\partial x_i \\ &= \overline{(S_d)}_s(-\partial\bar{c}/\partial x_i/\Sigma_{2D})\Sigma_{2D} = \frac{\overline{(S_d)}_s}{\overline{(S_{d2D})}_{s2}}\overline{(S_{d2D})}_{s2}\overline{(M_i)}_{s2}\Sigma_{2D}\end{aligned} \ , \tag{7a}$$

where $M_i = -\partial c/\partial x_i/\Sigma_2$ (with $i = 1$ and 2) is the flame normal vector in two-dimensional projection. Using eq. 6f and 4 one obtains:

$$\overline{(S_d N_i)}_s\Sigma_{gen} = \frac{\pi}{4}\overline{(S_{d2D})}_{s2}\overline{(M_i)}_{s2}\Sigma_{2D} \ . \tag{7b}$$

The propagation term in two-dimensions can be measured in the following manner if the measurement plane contains the mean direction of flame propagation (i.e. say m_1 direction):

$$P_{2D} = -\frac{\partial\overline{(S_{d2D})}_{s2}\overline{(M_{m_1})}_{s2}\Sigma_{2D}}{\partial x_{m_1}} \ . \tag{8a}$$

Similarly one can write the three-dimensional propagation term as:

$$P_{3D} = -\frac{\partial\overline{(S_d)}_s\overline{(N_{m_1})}_s\Sigma_{gen}}{\partial x_{m_1}} \ . \tag{8b}$$

Considering statistical homogeneity in the directions transverse to the flame propagation it may be possible to assume:

$$\frac{\partial(\overline{S_d})_s(\overline{N_{m_2}})_s\Sigma_{gen}}{\partial x_{m_2}} = \frac{\partial(\overline{S_d})_s(\overline{N_{m_3}})_s\Sigma_{gen}}{\partial x_{m_3}} = 0 \qquad (8c)$$

where m_2 and m_3 are mutually perpendicular directions normal to the m_1 direction and the coordinates along m_1, m_2 and m_3 directions are given by x_{m_1}, x_{m_2} and x_{m_3} respectively. Similarly, M_{m_1}, M_{m_2} and M_{m_3} are components of flame-normal vector in two-dimensions in m_1, m_2 and m_3 directions. This leads to the following expression:

$$\frac{\partial(\overline{S_{d2D}})_{s2}(\overline{M_{m_2}})_{s2}\Sigma_{2D}}{\partial x_{m_2}} = \frac{\partial(\overline{S_{d2D}})_{s2}(\overline{M_{m_3}})_{s2}\Sigma_{2D}}{\partial x_{m_3}} = 0 \ . \qquad (8d)$$

Based on eqs. 7b and 8b one obtains the following correction relation for the FSD propagation term:

$$P_{3D} = -\frac{\pi}{4}\left[\frac{\partial(\overline{S_{d2D}})_{s2}(\overline{M_{m_1}})_{s2}\Sigma_{2D}}{\partial x_{m_1}}\right]. \qquad (8e)$$

Relation between the three-dimensional curvature term and its two-dimensional projection

If h_3 denotes the height of the point P above the tangent plane (see Fig. 1a) it can be shown that [40,51]:

$$h_3 = \frac{1}{2}\kappa_1 y_{e1}^2 + \frac{1}{2}\kappa_2 y_{e2}^2 \ , \qquad (9a)$$

where y_{e1} and y_{e2} denote distances in principal directions e_1 and e_2 corresponding to the principal curvatures (i.e. κ_1 and κ_2) of the curvature tensor in the tangent plane at P. Based on Fig. 1 one finds:

$$h_2 \cos\phi = h_3 \ , \tag{9b}$$

where h_2 is the measured height above the tangent t_1 in the two-dimensional plane. If α is the angle between t_1 and e_1 directions, the distances y_{e1} and y_{e2} in the $\vec{e}$ reference frame are given by:

$$y_{e1} = y_{t1}\cos\alpha + y_{t2}\sin\alpha \quad \text{and} \quad y_{e2} = -y_{t1}\sin\alpha + y_{t2}\cos\alpha \ , \tag{9c}$$

where y_{t1} and y_{t2} are distances in the $\vec{t}$ reference frame. Accordingly the two-dimensional curvature is given by:

$$k_2 = \frac{1}{2}\frac{\partial^2 h_2}{\partial y_{t_1}^2} \ . \tag{9d}$$

Equations 9a-d can be used to obtain:

$$2k_2\cos\phi = \kappa_1\cos^2\alpha + \kappa_2\sin^2\alpha \ . \tag{9e}$$

Assuming isotropic distributions of ϕ and α one obtains:

$$2\overline{(k_2)}_{s2}\Sigma_{2D} = [\overline{\cos^2\alpha}\ \overline{(\kappa_1)}_s + \overline{\sin^2\alpha}\ \overline{(\kappa_2)}_s]\Sigma_{gen} \ . \tag{9f}$$

One obtains $\overline{\cos^2\alpha} = \overline{\sin^2\alpha} = 1/2$, if the angle α is assumed to be distributed uniformly between 0 and 2π. This gives rise to:

$$2\overline{(k_2)}_{s2}\Sigma_{2D} = 0.5[\ \overline{(\kappa_1)}_s + \overline{(\kappa_2)}_s]\Sigma_{gen} = \overline{(\kappa_m)}_s\Sigma_{gen} \ . \tag{9g}$$

Using eq. 4 one obtains:

$$\overline{(\kappa_m)}_s = \pi/2 \times \overline{(k_2)}_{s2} \ . \tag{9h}$$

Using eq. 9e the curvature-term in two-dimensions is given by:

$$2\overline{(S_{d2D}k_2)}_{s2}\Sigma_{2D} = 2\overline{(S_{d2D}k_2\Sigma_2)} = \overline{S_d \frac{(\kappa_1 \cos^2\alpha + \kappa_2 \sin^2\alpha)}{\cos^2\phi}\Sigma_3 \cos\phi} \ . \tag{10a}$$

Using statistical independence of α and ϕ with respect to other quantities, one obtains:

$$2\overline{(S_{d2D}k_2)}_{s2}\Sigma_{2D} = \overline{S_d \frac{(\kappa_1 \cos^2\alpha + \kappa_2 \sin^2\alpha)}{\cos\phi}\Sigma_3} = \overline{S_d\kappa_1\Sigma_3}\overline{\left(\frac{1}{\cos\phi}\right)}_s \overline{\cos^2\alpha} + \overline{S_d\kappa_2\Sigma_3}\overline{\left(\frac{1}{\cos\phi}\right)}_s \overline{\sin^2\alpha} \tag{10b}$$

Using $P(\phi)$ given by eq. 3f, one obtains $\overline{(1/\cos\phi)}_s = \pi/2$ and this along with $\overline{\cos^2\alpha} = \overline{\sin^2\alpha} = 1/2$ (considering the uniform distribution of α under the isotropic assumption) gives rise to:

$$2\overline{(S_{d2D}k_2)}_{s2}\Sigma_{2D} = \frac{\pi}{4}(\overline{S_d\kappa_1\Sigma_3} + \overline{S_d\kappa_2\Sigma_3}) = \frac{\pi}{4} \times 2\overline{(S_d\kappa_m)}_s\Sigma_{gen} \ . \tag{10c}$$

This provides the following correction to the curvature term measured in two-dimensions in order to obtain the curvature term in three-dimensions:

$$2\overline{(S_d\kappa_m)}_s\Sigma_{gen} = \frac{4}{\pi} \times 2\overline{(S_{d2D}k_2)}_{s2}\Sigma_{2D} \ . \tag{10d}$$

The relations between the two-dimensional and three-dimensional quantities relevant to the FSD transport are summarised in Table I for quick reference of the readers. The predictive capabilities of these expressions will be assessed based on the FSD transport related quantities extracted from DNS data in Section IV of this paper.

III. NUMERICAL IMPLEMENTATION

In the present study a DNS database of freely propagating statistically planar turbulent premixed flames under decaying turbulence has been considered. The simulation domain is taken to be a rectangular parallelepiped for all the simulations where the x_1-direction is taken to be the direction of mean flame propagation, whereas the other directions are considered to be periodic. The domain boundaries in the x_1-direction in case A are taken to be turbulent inlet and outlet respectively. The domain boundaries in the direction of mean flame propagation in other cases are taken to be partially non-reflecting. The partially non-reflecting boundaries are specified using the Navier Stokes Characteristic Boundary Condition (NSCBC) technique.[52] In case A, the spatial differentiation in the x_1-direction is carried out using the 6^{th} order central difference scheme for the internal grid points but the order of the differentiation gradually deceases to one-sided 4^{th} order difference scheme whereas the differentiation in the transverse directions are carried out using a spectral method. For the other cases, a 10^{th} order central-difference schemes is used for spatial discretisation for internal points which gradually decreases to a one-sided 2^{nd} order scheme near non-periodic boundaries. The time advancement for all viscous and diffusive terms in case A is carried out using an implicit solver, whereas the convection terms in case A and all the terms in all other cases are time advanced using a low-storage third order Runge-Kutta method.[53] For all cases, the flame is initialised by a steady unstrained planar laminar flame solution, and the initial velocity fluctuation field is specified by an initially homogeneous isotropic turbulence using a pseudo-spectral method.[54] The grid spacing is determined by the resolution of the flame structure, and about 10 grid points are kept within the thermal flame thickness $\delta_{th} = (T_{ad} - T_0) / Max\left|\nabla \hat{T}\right|_L$ for all cases considered here where T_{ad}, T_0 and $\hat{T}$ are the adiabatic flame temperature, unburned gas temperature and instantaneous gas temperature, respectively, and the subscript L refers to unstrained planar laminar flame quantities. The initial

values for the root-mean-square (rms) turbulent velocity fluctuation normalised by unstrained planar laminar burning velocity u'/S_L and the integral length scale to flame thickness ratio l/δ_{th} are presented in Table II along with the values of Damköhler number $Da = l.S_L/u'\delta_{th}$, Karlovitz number $Ka = (u'/S_L)^{3/2}(l/\delta_{th})^{-1/2}$, turbulent Reynolds number $\mathrm{Re}_t = \rho_0 u' l/\mu_0$, heat release parameter $\tau = (T_{ad} - T_0)/T_0$ and Lewis number Le. Standard values are taken for Prandtl number Pr, ratio of specific heats $\gamma = C_P/C_V$ and the Zel'dovich number $\beta = T_{ac}(T_{ad} - T_0)/T_{ad}^2$ (i.e. $\mathrm{Pr} = 0.7$, $\gamma = 1.4$, $\beta = 6.0$). It can be seen from Table II turbulent Reynolds numbers are comparable for cases A-G and I. Case A represents the corrugated flamelets regime combustion whereas other cases represent the thin reaction zones regime combustion.[49] The values of heat release parameters are different for cases A, B and C-L. Cases C-E and G represent combustion with non-unity Lewis number and in other cases characteristic Lewis number is taken to be unity. Five different values of Lewis number (i.e. *Le*= 0.34, 0.6, 0.8, 1.0 and 1.2 in cases C-G) have been considered here because some expressions relating the two-dimensional and three-dimensional FSD related quantities may work for all values of Lewis number, but other relations may perform satisfactorily only for Lewis numbers close to unity. The turbulent Reynolds number Re_t scales as $\mathrm{Re}_t \sim Da^2 Ka^2$, and thus the variation of turbulent Reynolds number in cases H-L is brought about by modifying the Damköhler and Karlovitz numbers independently of each other. In cases H, J and L the Damköhler number Da is held constant while the Karlovitz number Ka is held constant in cases I, J and K. Therefore, cases H-L are presented here to assesses the performance of the expressions relating the two-dimensional and three-dimensional quantities (eqs. 4, 6d, 7b, 8c and 10d) for different values of turbulent Reynolds number, irrespective of whether the change in Re_t is brought about by changing Da or Ka.

In all cases flame-turbulence interaction takes place under decaying turbulence. Under decaying turbulence, simulations should be carried out for at least $t_{sim} = Max(t_f, t_c)$, where $t_f = l/u'$ is the initial eddy turn over time and $t_c = \delta_{th}/S_L$ is the chemical time scale. The simulation in case A was run for about 4 initial eddy turn over times $(t_{sim} \sim 4\tau_f = 4l/u')$, whereas simulations were run for a time equal to $2.0t_f$ in case K; $3.0t_f$ in cases B-H, J, and L; and $4.34t_f$ for case I. The aforementioned simulation times remain either greater than (cases A) or equal to (cases B-L) one chemical time scale and are comparable to several previous studies.[4,9-11,14,44-48,55-58] The turbulent kinetic energy and its dissipation rate in the unburned gas ahead of the flame were not varying significantly with time when statistics were extracted and the qualitative nature of the statistics was found to have remained unchanged since $t = 1.5l/u'$ for all cases. The values of u'/S_L in the fresh reactants ahead of the flame at the time when statistics were extracted decreased by about 52% , 50%, 45%, 55% , 40%, 25% and 32% of the initial values in cases A, B-G, H, I, J, K and L, respectively. The values of l/δ_{th} have increased from their initial values by a factor of about 1.10, 1.7, 1.5-2.25 for cases A, B-G and H-L, respectively, but there are still enough turbulent eddies on each side of the computational domain.

The Reynolds/Favre averaged quantities are taken to be functions of the distance along the direction of mean flame propagation (x_1 direction), and are evaluated by ensemble averaging the relevant quantities in transverse directions ($x_2 - x_3$ planes). The statistical convergence of the Reynolds/Favre averaged quantities was assessed by comparing the corresponding values obtained using half of the sample size in the transverse directions using a distinct half of the

domain, with those obtained based on the full sample size. Both the qualitative and quantitative agreements between these sets of values were found to be satisfactory. In the next section, for the sake of brevity, only the results obtained based on full sample size will be presented.

IV. RESULTS & DISCUSSION

The relations between the two-dimensional and the corresponding three-dimensional quantities discussed in Section II will be assessed based on the analysis of DNS data in this section where both the two-dimensional and three-dimensional quantities are extracted from DNS database. In the present analysis all the relevant two-dimensional quantities were evaluated on every $x_1 - x_2$ and $x_1 - x_3$ plane so that the direction of mean flame propagation lies on the measurement plane. For statistically planar turbulent premixed flames the Favre-averaged reaction progress variable $\widetilde{c}$ remains a unique function of the spatial co-ordinate x_1 thus all the statistics in this section will be presented as a function of $\widetilde{c}$.

Behaviours of Σ_{gen} and Σ_{2D}

The variations of Σ_{gen}, Σ_{2D} and $4/\pi \times \Sigma_{2D}$ with $\widetilde{c}$ for cases A, B, C, and E-G are shown in Figs. 2a-f, respectively. The case D is not explicitly shown in Fig. 2 due to its qualitative similarity to other cases. It can be seen from Figs. 2a-f that the qualitative behaviours of Σ_{gen} and Σ_{2D} remain similar for all the cases. In all cases the maximum values of Σ_{gen} and Σ_{2D} are obtained slightly towards the unburned gas side of the middle of the flame brush (i.e. $\widetilde{c} < 0.5$). Comparing Figs. 2c-f reveals that the maximum values of Σ_{gen} and Σ_{2D} decrease with decreasing value of global Lewis number. The extent of flame wrinkling increases with

decreasing Lewis number especially for sub-unity Lewis numbers because of thermo-diffusive instabilities[42-48], which leads to higher extent of broadening of flame brush with decreasing Lewis number.

Comparing Figs. 2b and e reveals that the change in heat release parameter τ from 3.0 to 4.5 does not have any major influence on the maximum values of Σ_{gen} and Σ_{2D} when u'/S_L remains unchanged. Figure 2 also indicates that the maximum values of Σ_{gen} and Σ_{2D} for cases B-G are greater than in case A because the greater extent of flame wrinkling in cases B-G overcomes the broadening of flame brush thickness. However, it can be seen from Figs. 2a-f that the qualitative and quantitative agreement between Σ_{gen} and $(4/\pi)\times\Sigma_{2D}$ are excellent in all cases, which essentially indicates that the assumption of isotropic distribution of ϕ and its presumed surface area weighted pdf $P(\phi)$, as given by eq. 3f, remain valid for flames representing the corrugated flamelets and thin reaction zones regimes of turbulent premixed combustion for a large range of global Lewis number Le. Moreover, the heat release parameter τ does not seem to have any influence on the assumption of isotropy of ϕ and its presumed surface area weighted pdf $P(\phi)$ (eq. 3f).

Variations of Σ_{gen}, Σ_{2D} and $4/\pi\times\Sigma_{2D}$ with $\tilde{c}$ for cases H, J and L are shown in Figs. 3a-c, respectively (cases I and K are not shown here because of their qualitative similarities to cases H and L, respectively). Figures 3a-c indicate that the maximum values of Σ_{gen} and Σ_{2D} decrease slightly with increasing turbulent Reynolds number because the broadening of flame brush overcomes the greater extent of flame wrinkling at high values of u'/S_L. It can further be seen

from Figs. 3a-c that Σ_{2D} mimics the qualitative variation of Σ_{gen} for all the cases and the qualitative and quantitative agreement between Σ_{gen} and $(4/\pi)\times\Sigma_{2D}$ are excellent for these cases. This essentially substantiates that the assumption of isotropic distribution of ϕ and its presumed surface-area weighted pdf $P(\phi)$ given by eq. 3f are not significantly affected by the variations of turbulent Reynolds number in the range of Re_t considered in this study. It is expected that the isotropy assumption would improve at higher Reynolds number, which presumably covers many typical premixed combustion experiments.

Behaviours of $\overline{(a_T)}_s\Sigma_{gen}$ and $\overline{(a_{T2D})}_{s2}\Sigma_{2D}$

The variations of $\overline{(a_T)}_s\Sigma_{gen}$, $\overline{(a_{T2D})}_{s2}\Sigma_{2D}$ and $(8/\pi)\times\overline{(a_{T2D})}_{s2}\Sigma_{2D}$ with $\tilde{c}$ for cases A, B, C, E-G are shown Figs. 4a-f respectively. The same quantities for cases H, J and L are shown in Figs. 5a-c respectively. The cases D, I and K are not explicitly shown in Figs. 4 and 5 due to their qualitative similarities of the variations of $\overline{(a_T)}_s\Sigma_{gen}$, $\overline{(a_{T2D})}_{s2}\Sigma_{2D}$ and $(8/\pi)\times\overline{(a_{T2D})}_{s2}\Sigma_{2D}$ in cases C, H and L, respectively. It is evident that the tangential strain rate term $\overline{(a_T)}_s\Sigma_{gen}$ remains positive throughout the flame brush for all cases, which is consistent with several previous studies.[1-3,5,6,10-14] It can be seen from Figs. 4 and 5 that $\overline{(a_{T2D})}_{s2}\Sigma_{2D}$ remains qualitatively similar to, but smaller than, $\overline{(a_T)}_s\Sigma_{gen}$ throughout the flame brush. Figures 4 and 5 suggest that eq. 6d significantly underpredicts the magnitude of $\overline{(a_T)}_s\Sigma_{gen}$ for cases A and C-J but the agreement between the prediction of eq. 6d and the three-dimensional tangential strain rate term is satisfactory for cases B, K and L. This clearly indicates that the relation given by eq. 6d works well for higher values of turbulent Reynolds number Re_t and this agreement deteriorates with

decreasing Re_t (see Figs. 5a-e). It can be seen from Figs. 4c-f that the performance of eq. 6d also deteriorates with decreasing Lewis number. A comparison between Figs. 4a and b reveals that the level of disagreement between $(8/\pi)\times\overline{(a_{T2D})}_{s2}\Sigma_{2D}$ and $\overline{(a_T)}_s\Sigma_{gen}$ is greater for the flame representing the corrugated flamelets regime (case A) than in the flame with comparable values of turbulent Reynolds number and heat release parameter representing the thin reaction zones regime combustion (i.e. case B). It can be seen by comparing Figs. 4b and f that eq. 6d almost accurately captures the quantitative behaviour of $\overline{(a_T)}_s\Sigma_{gen}$ for case B (i.e. $(8/\pi)\times\overline{(a_{T2D})}_{s2}\Sigma_{2D}$ slightly overpredicts $\overline{(a_T)}_s\Sigma_{gen}$ towards the unburned gas side of the flame brush) whereas eq. 6d underpredicts $\overline{(a_T)}_s\Sigma_{gen}$ in case F. This essentially suggests that eq. 6d starts to work better at smaller values of turbulent Reynolds number for flames with small values of heat release parameter τ.

The reason for the difference between $(8/\pi)\times\overline{(a_{T2D})}_{s2}\Sigma_{2D}$ and $\overline{(a_T)}_s\Sigma_{gen}$ can be explained in the following manner. It was assumed that $\cos\phi$ is independent of a_T while deriving eq. 6d. However, this might not be true for the cases where effects of heat release are dominant. The scalar gradient aligns preferentially with the most compressive strain rate for usual passive scalar mixing whereas in turbulent premixed flames the alignment of reaction progress variable gradient ∇c depends on the competition between the strain rate a_{chem} induced by chemical heat release and turbulent straining a_{turb}.[59-61] It has been shown that ∇c preferentially aligns with the most extensive (compressive) principal strain rate when a_{chem} (a_{turb}) dominates over a_{turb} (a_{chem}).[59-61] It has been shown by Chakraborty and Swaminathan[59] and Chakraborty *et al.*[61] the ratio

a_{chem}/a_{turb} can be scaled as $a_{chem}/a_{turb} \sim \tau\, f(Le)Da \sim \tau\, f(Le)\mathrm{Re}_t^{1/2}/Ka$ where $f(Le)$ is a function of Lewis number which increases with decreasing Le. This essentially suggests that the effects of a_{chem} strengthen with decreasing Lewis number Le and with increasing values of heat release parameter τ and Damköhler number Da. Alternatively, it can be said that the effects of a_{chem} strengthen with increasing $\mathrm{Re}_t \sim Da^2Ka^2$ when Ka is held constant. On the other hand a_{turb} dominates over the effects of a_{chem} for large values of Ka when Re_t is held constant. The alignment of ∇c with local principal strain rate affects the statistics of tangential strain rate which can be elucidated by writing the tangential strain rate $a_T = (\delta_{ij} - N_iN_j)\partial u_i/\partial x_j$ in the following manner:

$$a_T = \partial u_j/\partial x_j - N_iN_j\partial u_i/\partial x_j = e_\alpha(1-\cos^2\theta_\alpha) + e_\beta(1-\cos^2\theta_\beta) + e_\gamma(1-\cos^2\theta_\gamma)\ , \qquad (11a)$$

where e_α, e_β and e_γ are the most extensive, intermediate and most compressive principal strain rates respectively and angles θ_α, θ_β and θ_γ are the angles between ∇c and the principal directions corresponding to e_α, e_β and e_γ respectively. It is reasonable to assume that the principal direction corresponding to e_α aligns with the mean direction of flame propagation (i.e. x_1 direction) for small values of u'/S_L where the flame is weakly wrinkled under turbulence. Under this condition, $\cos\theta_\alpha$ can be estimated as:

$$\cos\theta_\alpha \approx M_1\cos\phi\ , \qquad (11b)$$

where M_1 is the component of the apparent flame-normal on the measurement plane in the direction of mean flame propagation. Equation 11b demonstrates that a_T cannot be taken independent of $\cos\phi$ when the direction cosines corresponding to the principal direction with which ∇c preferentially aligns becomes a function of the angle ϕ and this situation is prevalent

when ∇c aligns with the most extensive principal strain rate. Under this situation the approximation $\overline{(a_T \cos\phi)}_s = \overline{(a_T)}_s \cdot \overline{(\cos\phi)}_s$ used in eq. 6c is rendered invalid and thus eq. 6d cannot be taken to relate $\overline{(a_{T2D})}_{s2}\Sigma_{2D}$ with the actual three-dimensional tangential strain rate term $\overline{(a_T)}_s\Sigma_{gen}$. The angle θ_γ is expected to be randomly orientated with respect to the angle ϕ when ∇c aligns with the most compressive principal strain rate and under this condition the approximation $\overline{(a_T \cos\phi)}_s = \overline{(a_T)}_s \cdot \overline{(\cos\phi)}_s$ is expected to be valid and thus eq. 6d is likely to relate the quantities $\overline{(a_T)}_s\Sigma_{gen}$ and $\overline{(a_{T2D})}_{s2}\Sigma_{2D}$ in a satisfactory manner. The above explanations can be substantiated from the observations made from Figs. 4 and 5. In cases A and C-E, the reaction progress variable gradient ∇c aligns predominantly with e_α (Refs. 59, 61) and thus the relation given by eq. 6d does not work well in these cases. However, the extent of ∇c alignment with e_α decreases with increasing Lewis number and thus the difference between $(8/\pi)\times\overline{(a_{T2D})}_{s2}\Sigma_{2D}$ and $\overline{(a_T)}_s\Sigma_{gen}$ decreases from case C to case G (see Figs. 4c-f). The extent of ∇c alignment with e_α in case F is greater than in case B due to greater value of τ in case F and thus eq. 6d underpredicts the magnitude of $\overline{(a_T)}_s\Sigma_{gen}$ in case F whereas predicts the magnitude of $\overline{(a_T)}_s\Sigma_{gen}$ satisfactorily in case B. Although cases A and B have comparable τ and Re_t, the value of Da is much greater in case A than in case B, which gives rise significantly greater extent of ∇c alignment with e_α in case A than in case B. As a result of this, eq. 6d does not work well in case A but works satisfactorily in case B. For high values of $u'/S_L \sim \mathrm{Re}_t^{1/4} Ka^{1/2}$, the flame becomes highly wrinkled as a result the relation between $\cos\theta_\alpha$ and $\cos\phi$ can no longer be correlated by eq. 11b (i.e. the e_α direction may not coincide with the

mean direction of flame propagation) and this essentially is reflected in the weak correlation between $\cos\theta_\alpha$ and $\cos\phi$ for high values of Re_t and Ka. As a result of this, the relation given by eq. 6d works well for higher values of Re_t and Ka irrespective of Damköhler number because $\overline{(a_T\cos\phi)}_s$ can be accurately approximated by $\overline{(a_T)}_s\cdot\overline{(\cos\phi)}_s$ when a_T and $\cos\phi$ are uncorrelated with other. This can be substantiated by comparing Figs. 5a-c for cases H, J and L, which show that eq. 6d works well for the cases with high values of turbulent Reynolds number Re_t.

Behaviours of the two-dimensional and three-dimensional propagation terms (P_{2D} and P_{3D})

In the context of statistically planar flames with mean direction of flame propagation aligned with x_1-direction, the propagation term in two-dimensions and three-dimensions take the forms $-\partial[\overline{(S_{d2D})}_{s2}\overline{(M_1)}_{s2}\Sigma_{2D}]/\partial x_1$ and $-\partial[\overline{(S_dN_1)}_s\Sigma_{gen}]/\partial x_1$ respectively. This essentially indicates that the interrelation between $\overline{(S_{d2D})}_{s2}\overline{(M_1)}_{s2}\Sigma_{2D}$ and $\overline{(S_dN_1)}_s\Sigma_{gen}$ is the key for linking P_{2D} with P_{3D}. The variations of $\overline{(S_{d2D})}_{s2}\overline{(M_1)}_{s2}\Sigma_{2D}$ and $\overline{(S_dN_1)}_s\Sigma_{gen}$ with $\tilde{c}$ for cases A-C, E, G, I-K are shown in Figs. 6a-h, respectively. The cases D, F, H, and L are not shown because of their qualitative similarities with cases C, J, I and K, respectively. In all cases $\overline{(S_{d2D})}_{s2}\overline{(M_1)}_{s2}\Sigma_{2D}$ overpredicts the magnitude of $\overline{(S_dN_1)}_s\Sigma_{gen}$ in spite of capturing the correct qualitative behaviour. It can be seen from Figs. 6a-h that the correction given by eq. 7b (i.e. $\overline{(S_dN_1)}_s\Sigma_{gen} = \pi/4\times\overline{(S_{d2D})}_{s2}\overline{(M_1)}_{s2}\Sigma_{2D}$) satisfactorily predicts $\overline{(S_dN_1)}_s\Sigma_{gen}$ for all the cases considered here.

The relation given by eq. 7b relies on the relation between Σ_{gen} and Σ_{2D} (i.e. eq. 6d). The relation between Σ_{gen} and Σ_{2D} according to eq. 6d is based on that the assumption of isotropic distribution of ϕ and its presumed surface area weighted pdf $P(\phi)$, as given by eq. 3f. It has been shown in Figs. 2 and 3 that these assumptions remain valid for all the flames considered here. As a result of this eq. 7b also satisfactorily relates $\overline{(S_{d2D})}_{s2}\overline{(M_1)}_{s2}\Sigma_{2D}$ and $\overline{(S_d N_1)}_s\Sigma_{gen}$ for all the cases considered in this study.

Behaviours of the two-dimensional and three-dimensional curvature terms

The variations of $\overline{(\kappa_m)}_s$ and $\overline{(k_2)}_{s2}$ with $\tilde{c}$ for cases A-C, E, G, I-K are shown in Figs. 7a-h respectively. The cases D, F, H and L are not shown for their qualitative similarities with cases C, J, I and K respectively. It can be seen that both $\overline{(\kappa_m)}_s$ and $\overline{(k_2)}_{s2}$ remain positive towards the unburned gas side and before assuming negative values towards the burned gas side of the flame brush. Although $\overline{(k_2)}_{s2}$ captures the qualitative behaviour of $\overline{(\kappa_m)}_s$ it underpredicts the magnitude of $\overline{(\kappa_m)}_s$. It is clear from Fig. 7 that $\pi/2\times\overline{(k_2)}_{s2}$ predicts $\overline{(\kappa_m)}_s$ accurately for all the cases considered here (according to eq. 9h), which essentially suggests that the assumptions of isotropy of the distributions of the angles ϕ and α and the pdf $P(\phi)$, as given by eq. 3f, remain approximately valid for all the cases irrespective the values of τ, Le, Re_t and regime of combustion.

The variations of two-dimensional and three-dimensional FSD curvature terms (i.e. $2\overline{(S_{d2D}k_2)}_{s2}\Sigma_{2D}$ and $2\overline{(S_d\kappa_m)}_s\Sigma_{gen}$) with $\tilde{c}$ for cases A, B, C, E-G are shown Figs. 8a-f

respectively. These variations for cases H, J and L are shown in Figs. 9a-c respectively. The cases D, I and K are not explicitly shown in Figs. 8 and 9 due to their qualitative similarities to cases C, H and L, respectively. For all cases, $2\overline{(S_{d2D}k_2)}_{s2}\Sigma_{2D}$ captures the qualitative behaviour of $2\overline{(S_d\kappa_m)}_s\Sigma_{gen}$ but underpredicts its magnitude. It can be seen from Figs. 8c-f that the curvature term in both two- and three-dimensions assumes positive values towards the unburned gas side of the flame brush before becoming negative towards the burned gas side for the flames with low Lewis number (i.e. cases C and E). However, the magnitude of positive (negative) contribution of the curvature term decreases (increases) with increasing Lewis number Le (see Figs. 8c-f). Comparing Figs. 8b and e it is evident that τ does not have any major effect on the qualitative behaviour of the FSD curvature term $2\overline{(S_d\kappa_m)}_s\Sigma_{gen}$ for the unity Lewis number flames (i.e. cases B and F). Figures 9a-c show that the curvature term $2\overline{(S_d\kappa_m)}_s\Sigma_{gen}$ remains principally negative for the different values of turbulent Reynolds number for the unity Lewis number flames (i.e. cases H, J and L) although weak positive values have been observed towards the unburned gas side of the flame brush for cases H and I.

It can be seen from Figs. 8 and 9 that $(4/\pi)\times 2\overline{(S_{d2D}k_2)}_{s2}\Sigma_{2D}$ underpredicts the magnitude of the FSD curvature term for low and moderate turbulent Reynolds number cases with Lewis number close to unity (e.g. cases A,B, E-G and H-J). However, eq. 10d predicts the three-dimensional FSD curvature term satisfactorily for the flames in the thin reaction zones regime flames with high turbulent Reynolds number (e.g. cases K and L) or with Lewis number much smaller than unity (e.g. cases C and D). This suggests that the relation given by eq. 10d starts to

work satisfactorily for smaller values of turbulent Reynolds number when the flames represent the thin reaction zones regime combustion with Lewis number significantly smaller than unity.

It was assumed while deriving eq. 10d that angles α and ϕ are uncorrelated with each other and independent of other quantities. However, this essentially indicates that the correlations between S_{d2D} and k_2 and between Σ_2 and k_2 are identical to the correlations between S_d and κ_m and between Σ_3 and κ_m. The correlation coefficients between S_d and κ_m (S_{d2D} and k_2) and between Σ_3 and κ_m (Σ_2 and k_2) for different c isosurfaces across the flame brush are presented in Table III (Table IV). It can be seen from Tables III and IV that S_d and κ_m are negatively correlated for all the flames throughout the flame brush but the correlation coefficients between S_d and κ_m are significantly different from the correlation coefficients between S_{d2D} and k_2. However, the correlation between S_d and κ_m becomes weak for small Le flames for a given set of values of Re_t, Da and Ka (see cases C-G). Moreover, this correlation weakens with increasing Re_t when either Da or Ka is held constant for a given value of Le (see cases H-L). The curvature dependence of S_d in the flame (i.e. case A) representing the corrugated flamelets regime remains weaker than in the flames representing the thin reaction zones regime combustion at comparable values of turbulent Reynolds number (i.e. cases B and F), which is consistent with the scaling analysis of Peters[49] and previous DNS results.[62] It can be seen from Tables III and IV that the correlation coefficients between Σ_3 and κ_m is different from the correlation coefficients between Σ_2 and k_2. In the $Le = 1.2$ flame (i.e. case G), Σ_3 and κ_m are negatively correlated whereas this correlation is positive for the flames with $Le < 1$ (i.e. cases C-E) and in case A (i.e. the case representing the corrugated flamelets regime combustion). For all

the $Le = 1.0$ thin reaction zones regime flames (i.e. cases B, F, H-I) Σ_3 and κ_m remain weakly correlated with each other whereas the correlation between Σ_3 and κ_m remain strongly positive in the unity Lewis number flame representing the corrugated flamelets regime (i.e. case A). From the above discussion it is evident that negative correlation between S_d and κ_m is partially nullified by the positive correlation between Σ_3 and κ_m for the $Le < 1$ flames (i.e. case C-E), whereas the negative $S_d - \kappa_m$ correlation is aided by the negative $\Sigma_3 - \kappa_m$ correlation in the $Le > 1$ case (i.e. case G). As correlation coefficients between S_{d2D} and k_2 (Σ_2 and k_2) are different from those between S_d and κ_m (Σ_3 and κ_m) the relation between $2\overline{(S_{d2D}k_2)}_{s2}\Sigma_{2D}$ and $2\overline{(S_d\kappa_m)}_s\Sigma_{gen}$ cannot be just accounted for by a constant multiplier as suggested by eq. 10d for the cases where the effects of the correlations between S_d and κ_m and between Σ_3 and κ_m are relatively strong. As a result of this, $(4/\pi)\times 2\overline{(S_{d2D}k_2)}_{s2}\Sigma_{2D}$ underpredicts the magnitude of the FSD curvature term for low and moderate turbulent Reynolds number cases with Lewis number close to unity (i.e. cases A, B, E-G, H-J). As the correlation between S_d and κ_m are relatively weak in cases C, D, K and L, the difference between the $S_d - \kappa_m$ and $S_{d2D} - k_2$ correlations does not play any major role and thus eq. 10d satisfactorily relates the FSD curvature terms in two and three dimensions (i.e. $2\overline{(S_{d2D}k_2)}_{s2}\Sigma_{2D}$ and $2\overline{(S_d\kappa_m)}_s\Sigma_{gen}$). This essentially suggests that the success of the relation given by eq. 10d will be dependent on the values of turbulent Reynolds number, global Lewis number and the regime of the prevailing combustion process.

V. CONCLUSIONS

The predictions of the relations between two-dimensional projections of the different terms of the Reynolds averaged FSD transport equation and their corresponding actual three-dimensional counterparts derived based on isotropy assumptions by Hawkes *et al.*[40] are assessed using three-dimensional compressible DNS data of freely propagating statistically planar turbulent premixed flames under decaying turbulence with wide variations of Karlovitz number Ka, Lewis number Le, heat release parameter τ and turbulent Reynolds number Re_t. The main findings are summarised below:

- Based on the assumption of the isotropy of the angle between the normal vectors on the local flame surface and the measurement plane (Ref. 40), a simple algebraic relation (i.e. eq. 4) is derived which satisfactorily relates the generalised FSDs evaluated in two and three dimensions (i.e. Σ_{2D} and $\Sigma_{3D} = \Sigma_{gen}$) irrespective of the values of Ka, τ, Le and Re_t (see Figs. 2 and 3).
- The relations between the two-dimensional and three-dimensional counterparts of the surface-averaged curvature and the FSD propagation term (see eqs. 9h, 7b and 8e, and refer to Figs. 6 and 7) are also found to work well for all the values of Ka, τ, Le and Re_t considered in this study.
- The relation (i.e. eq. 6d) between the actual three-dimensional tangential strain rate term in the FSD transport equation and its two-dimensional projection, which is derived based on the assumption of isotropy, does not work well for small values of turbulent Reynolds number Re_t. The disagreement between the corrected two-dimensional tangential strain rate term and the actual three-dimensional strain rate term increases with increasing value of heat release parameter τ and decreasing Lewis number Le for same set of values of turbulent Reynolds,

Damköhler and Karlovitz numbers (see Figs. 4 and 5). This suggests that the threshold value of Re_t above which the assumption of isotropy is valid for the tangential strain rate term depends on the value of τ and Le.

- Moreover, the relation (i.e. eq. 6d) between the tangential strain rate term in the FSD transport equation based on two-dimensional projection and its actual value obtained based on isotropy performs relative poorly for the flames representing the corrugated flamelets regime of combustion. However, the same relation works reasonably well for a thin reaction zones regime flame with comparable values of turbulent Reynolds number and heat release parameter (see Figs. 4a and b).
- It has been found that the relation between the two and three dimensional curvature terms based on isotropy arguments (i.e. eq. 10d) underpredicts the magnitude of the FSD curvature term for low and moderate turbulent Reynolds number cases with Lewis number close to unity (see Figs. 8 and 9). However, the relation given by eq. 10d predicts the three-dimensional FSD curvature term satisfactory for the thin reaction zones regime flames with high turbulent Reynolds number or with Lewis number much smaller than unity (sees Figs. 8 and 9).

Detailed physical explanations have been provided for the disagreement between the prediction of the relations derived based on isotropy argument for both the tangential strain rate and curvature terms of the FSD transport equation. These physical arguments suggest that the relations between two and three dimensional values derived based on isotropy for the tangential strain rate and curvature terms work well for high values of turbulent Reynolds number but the

threshold value of Re_t above which the assumption of isotropy yields accurate result depends on the values of heat release parameter, Lewis number and the regime of the prevailing combustion process.

It is worth noting that the present analysis is carried out for a canonical configuration so that effects of τ, Le and Re_t on the performance of the expressions given by eqs. 4, 6d, 7b, 8e and 10d, which relate the actual three-dimensional FSD variables with the corresponding two-dimensional projections, can be assessed based on an extensive parametric study without exorbitant computational cost. The relations between two-dimensional and actual three-dimensional FSD and the terms of its transport equation (see Table I) are derived based on the assumption of isotropy which is independent of flow geometry in question. For high values of Re_t the turbulent conditions at the molecular scale (e.g. Kolmogorov or Gibson length scale) are likely to be isotropic irrespective of the flow configuration and as most chemical reaction occurs at the molecular scale, the isotropic relations derived in this paper are likely to work well for real burners (at least away from the burner exit) at high values of Re_t especially in the thin reaction zones regime where turbulent velocity fluctuations tend to mask the effects of flame normal acceleration. It was shown in Ref. 40 that the relations given in Table I work satisfactorily for the thin reaction zone regime flames in turbulent Bunsen-burner configuration at high values of Re_t. However, the present analysis indicates that the threshold value of Re_t, above which the relations based on the assumption of isotropy are likely to provide accurate results, depends on the mixture (which determines τ and Le) but the expressions which relate relevant two-dimensional quantities with the corresponding three-dimensional counterparts work satisfactorily

in the thin reaction zones regime when Re_t remains of the order of 100 for unity Lewis number flames. In real burners Re_t often assumes values much greater than 100, and thus the expressions which relate the actual three-dimensional FSD and the terms of its transport equation with the corresponding two-dimensional projections can be used to extract the three-dimensional information from the two-dimensional measurements, especially for hydrocarbon flames with global Lewis number close to unity.

ACKNOWLEDGEMENTS

NC gratefully acknowledges the practical help provided by Dr. Markus Klein and the financial support of ESPRC is also gratefully acknowledged. EH gratefully acknowledges the support of the Australian Research Council under the Future Fellowships program, grant number FT100100536.

REFERENCES

[1]R.S. Cant, S. B. Pope, and K.N.C. Bray, "Modelling of flamelet surface to volume ratio in turbulent premixed combustion", *Proc. of Comb. Inst.*, **23**, 809 (1990).

[2]S. Candel, D.Venante, F. Lacas, E. Maistret, N. Darabhia and T. Poinsot, "Coherent Flamelet Model: Applications and recent extensions", in *Recent Advances in Combustion Modelling*, ed. B.E. Larrouturou, World Scientific, Singapore, 19 (1990).

[3]J.M. Duclos, D. Veynante and T. Poinsot, "A comparison of flamelet models for turbulent premixed combustion", *Combust. Flame*, **95,**101 (1993).

[4]M. Boger, D. Veynante, H. Boughanem, and A. Trouvé, "Direct Numerical Simulation analysis of flame surface density concept for Large Eddy Simulation of turbulent premixed combustion", *Proc. of Combust. Inst.*, **27**, 917 (1998).

[5]E.R. Hawkes and R.S. Cant, "A flame surface density approach to large eddy simulation of premixed turbulent combustion", *Proc. of Combustion Inst.*, **28**, 51 (2000).

[6]E.R. Hawkes, and R.S. Cant, "Physical and numerical realizability requirements for flame surface density approaches to large-Eddy and reynolds averaged simulation of premixed turbulent combustion", *Combust. Theory Modelling*, **5**, 699 (2001).

[7] R. Knikker, D. Veynante and C. Meneveau, "A-priori testing of a similarity model for large eddy simulations of turbulent premixed combustion", *Proc. of Combust. Inst.*, **29**, 2105 (2005).

[8]S. Richard, O. Colin, O. Vermorel, A. Benkenida, C. Angelberger, D. Veynante, "Towards large eddy simulation of combustion in spark ignition engines", *Proc. Combustion Inst.*, 31 3059 (2009).

[9]N. Chakraborty, and R.S. Cant, "*A-Priori* Analysis of the Curvature and Propagation terms of the Flame Surface Density Transport Equation for Large Eddy Simulation", *Phys. Fluids,* **19**,105101 (2007).

[10]N. Chakraborty, M. Klein, "*A Priori* Direct Numerical Simulation assessment of algebraic Flame Surface Density models for turbulent premixed flames in the context of Large Eddy Simulation." *Phys. Fluids*, **20**, 085108(2008).

[11]N. Chakraborty, R.S. Cant, "Direct Numerical Simulation analysis of the Flame Surface Density transport equation in the context of Large Eddy Simulation." *Proc. of Combust. Inst.*, **32**, 1445 (2009).

[12]A. Trouvé and T.J. Poinsot, "The evolution equation for flame surface density in turbulent premixed combustion", *J. Fluid Mech*., **278**,1(1994).

[13] I. Han, I., K.H. Huh, "Roles of displacement speed on evolution of flame surface density for different turbulent intensities and Lewis numbers for turbulent premixed combustion", *Combust. Flame*, **152**, 194 (2008).

[14]M. Katragadda, S. P. Malkeson, N. Chakraborty, "Modelling of the tangential strain rate term of the Flame Surface Density Transport Equation in the context of Reynolds Averaged Navier Stokes Simulation", *Proc. Combust. Inst.*, **33**, 1429.

[15]D.Veynante, J.M. Duclos and J.Piana, "Experimental analysis of flamelet models for premixed turbulent combustion", *Proc. of Combust. Inst.*, **25**,1249 (1994).

[16]D.Veynante, J.Piana, J.M.Duclos, and C. Martel, "Experimental analysis of flame surface density models for premixed turbulent combustion", *Proc. of Combust. Inst.*, **26**,413(1996).

[17]J.F. Driscoll,"Flamelet structure and its effect on turbulent burning velocities, *Prog. Energy Combust. Sci*., **34**, 91 (2008).

[18]J. Hult, S. Gashi, N. Chakraborty, M. Klein, K.W. Jenkins, R.S. Cant, C. Kaminski, "Measurement of Flame Surface Density for Turbulent Premixed Flames using PLIF and DNS". *Proc. of Combust. Inst.*, **31**, 1319 (2007).

[19]A. M. Steinberg, J. F. Driscoll, "Stretch-rate relationships for turbulent premixed combustion LES subgrid models measured using temporally resolved diagnostics", *Combust. Flame*, 156, 2285 (2009).

[20]S. A. Filatyev, J. F. Driscoll, C. D. Carter, J. M. Donbar, "Simultaneous stereo particle image velocimetry and double-pulsed planar laser-induced fluorescence of turbulent premixed flames", *Combust. Flame*, **141**,1 (2005).

[21]I. G. Shepherd, W. T. Ashurst, "Flame front geometry in premixed turbulent flames", *Proc. Combustion Inst.*, 24, 485(1992).

[22]B. M. Deschamps, G. J. Smallwood, J. Prieur, D. R. Snelling, O. Gulder, "Surface density measurements of turbulent premixed flames in a spark-ignition engine and a bunsen-type burner using planar laser-induced fluorescence", *Proc. Combustion. Inst.*, 26, 427 (1996).

[23]S. S. Shy, E. I. Lee, N. W. Chang, S. I. Yang, Direct and indirect measurements of flame surface density, orientation, and curvature for premixed turbulent combustion modeling in a cruciform burner, *Proc. Combustion Inst.*, 28, 383(2000).

[24]I. G. Shepherd, R. K. Cheng, "The burning rate of premixed flames in moderate and intense turbulence", *Combust. Flame*, 127, 2066 (2001).

[25]Y. C. Chen, R. W. Bilger, "Experimental investigation of three-dimensional flame-front structure in premixed turbulent combustion—I: hydrocarbon/air bunsen flames", *Combust. Flame*, 131, 400(2002).

[26]T. Lachaux, F. Halter, C. Chauveau, I. Gokalp, I. G. Shepherd, “Flame front analysis of high-pressure turbulent lean premixed methane–air flames”, *Proc. Combustion Inst.*, 30 819 (2005).

[27]S. Gashi, J. Hult, K. W. Jenkins, N. Chakraborty, R. S. Cant, C. F. Kaminski, “Curvature and wrinkling of premixed flame kernels—comparisons of OH PLIF and DNS data”,*Proc. Combustion Inst.*, 30, 809 (2005).

[28]P. Anselmo-Filho, S. Hochgreb, R. S. Barlow, R. S. Cant, “Experimental measurements of geometric properties of turbulent stratified flames”, *Proc. Combustion Inst.*, 32 1763 (2009).

[29]F. Halter, C. Chauveau, I. Gokalp, D. Veynante, “Analysis of flame surface density measurements in turbulent premixed combustion”, *Combust. Flame*, 156, 657(2009).

[30] B.Renou, A.Boukhalfa, D.Peuchberty and M. Trinité, “Effects of stretch on the local structure of freely propagating premixed low-turbulent flames with various Lewis numbers”, *Proc. of Combust. Inst.*, **27**, 841(1998).

[31]D. Bradley, P. H. Gaskell, A. Sedaghat, X. J. Gu, “Generation of PDFS for flame curvature and for flame stretch rate in premixed turbulent combustion”, *Combust. Flame*, 135, 503 (2003).

[32]A. Soika, F. Dinkelacker, and A. Leipertz,“Measurement of resolved flame structure with constant Reynolds number”, *Proc. Combust. Inst.*, **27**,785 (1998).

[33]Y. C. Chen, M. Kim, J. Han, S. Yun, Y. Yoon, Measurements of the heat release rate integral in turbulent premixed stagnation flames with particle image velocimetry, *Proc. Combust. Inst.*, 31,1327 (2007).

[34]F. Halter, C. Chauveau, I. Gokalp, “Investigations on the Flamelet Inner Structure of Turbulent Premixed Flames”, *Combust. Sci. Tech.*, 180, 713 (2008).

[35]V. Robin, A. Mura, M. Champion, O. Degardin, B. Renou, M. Boukhalfa, “Experimental and numerical analysis of stratified turbulent V-shaped flames” ,*Combust. Flame*, 153,288(2008).

[36]I. F. Huang, S. S. Shy, C. C. Chang, S. C. Li, C. M. Huang, Spatiotemporal measurements of flame stretch and propagation rates for lean and rich CH_4/air premixed flames interacting with a turbulent-wake, *Proc. Combust. Inst.*, 32, 1755 (2009).

[37]B. Böhm, C. Heeger, I. Boxx, W. Meier, A. Dreizler, "Time-resolved conditional flow field statistics in extinguishing turbulent opposed jet flames using simultaneous highspeed PIV/OH-PLIF", *Proc. Combust. Inst.*, 32, 1647 (2009).

[38]D. A. Knaus, S. S. Sattler, F. C. Gouldin, "Three-dimensional temperature gradients in premixed turbulent flamelets via crossed-plane Rayleigh imaging", *Combust. Flame*, 141,253 (2005).

[39]S.S. Shy, W.K.E.I. Lee, T.S. Yang, "Experimental analysis of flame surface density modeling for premixed turbulent combustion using aqueous autocatalytic reactions", *Combust. Flame*, 118, 608 (1999).

[40]E.R. Hawkes, R. Sankaran, J. H. Chen, "Estimates of the three-dimensional Flame Surface Density and every term in its transport equation from two-dimensional measurements", *Proc. Combust. Inst.*, **33**, 1447.

[41]R. Sankaran, E. R. Hawkes, J. H. Chen, T. Lu and C. K. Law, "Structure of a spatially developing turbulent lean methane–air Bunsen flame", *Proc. Combust. Inst. ,* **31,** 1291 (2007).

[42]G.I. Sivashinsky, "Diffusional-thermal theory of cellular flames",*Combust. Sci. Tech.,* **16**,137 (1977).

[43] P.Clavin and F.A.Williams, "Effects of Molecular Diffusion and thermal expansion on the structure and dynamics of turbulent premixed flames in turbulent flows of large scale and small intensity", *J.Fluid Mech.,* **116**,251 (1982).

[44] D.C.Haworth and T.J.Poinsot, "Numerical simulations of Lewis number effects in turbulent premixed flames", *J.Fluid Mech*., **244**,405(1992).

[45] C.J.Rutland and A. Trouvé, "Direct Simulations of Premixed Turbulent Flames with Nonunity Lewis numbers",*Combust. Flame*, **94**,41 (1993).

[46] N. Chakraborty and R.S.Cant, "Influence of Lewis Number on Curvature Effects in Turbulent Premixed Flame Propagation in the Thin Reaction Zones Regime", *Phys. Fluids*, **17**,105105, (2005).

[47]N. Chakraborty, M. Klein, "Influence of Lewis number on the Surface Density Function transport in the thin reaction zones regime for turbulent premixed flames", *Phys. Fluids*, 20, 065102 (2008).

[48]N. Chakraborty, R.S. Cant, "Effects of Lewis number on scalar transport in turbulent premixed flames", *Physics Fluids*, 21, 035110 (2009).

[49] N. Peters, *Turbulent Combustion* (Cambridge University press, Cambridge, UK (2000).

[50]J.H. Chen, A. Choudhary, B. de Supinski,M.DeVries, E. R. Hawkes, S. Klasky, W. K. Liao, K. L. Ma, J. Mellor-Crummey, N. Podhorski, R. Sankaran, S. Shende, and C. S. Yoo, "Terascale direct numerical simulations of turbulent combustion using S3D", *Computational Science & Discovery*, 2, 015001, (2009)

[51]S.B.Pope, "The evolution of surfaces in turbulence", *Int. J. Engng. Sci*., **26**, 5, 445(1988).

[52]T. Poinsot, S.K. Lele, "Boundary conditions for direct simulation of compressible viscous flows", *J. Comp. Phys*., **101**, 104 (1992).

[53]A.A Wray, "Minimal storage time advancement schemes for spectral methods", NASA Ames Research Center, California, Report No. MS 202 A-1 (1990).

[54]R.S.Rogallo,*"Numerical experiments in homogeneous turbulence"*, NASA Technical Memorandum 91416, NASA Ames Research Center, California (1981).

[55]T.Echekki and J.H.Chen, "Unsteady Strain rate and Curvature Effects in Turbulent Premixed Methane-Air Flames",*Combust. Flame*, **116**,184 (1996).

[56] J.H.Chen and H.G.Im, "Correlation of Flame Speed with Stretch in Turbulent Premixed Methane/Air Flames",*Proc. of Combust. Inst.*, **27**,920 (1998).

[57]N.Peters, P.Terhoeven, J.H.Chen and T.Echekki, "Statistics of Flame Displacement Speeds from Computations of 2-D Unsteady Methane-Air Flames", *Proc. of Combust. Inst.*, **27**,833(1998).

[58]H.G.Im, and J.H.Chen, "Preferential diffusion effects on the burning rate of interacting turbulent premixed Hydrogen-Air flames", *Combust. Flame*, **131**, 246 (2002).

[59]N. Chakraborty, N. Swaminathan, "Influence of Damköhler number on Turbulence-Scalar interaction in Premixed Flames, Part I: Physical Insight." *Phys. Fluids*, 19, 045103 (2007).

[60]N. Chakraborty, J.W. Rogerson, N. Swaminathan, "*A-Priori* assessment of closures for scalar dissipation rate transport in turbulent premixed flames using direct numerical simulation", *Phys. Fluids*, 20,045106 (2008).

[61]N. Chakraborty, M. Klein, N. Swaminathan, "Effects of Lewis number on reactive scalar gradient alignment with local strain rate in turbulent premixed flames." *Proc. of Combust. Inst.*, 32,1409 (2009).

[62] N. Chakraborty, "Comparison of displacement speed statistics of turbulent premixed flames in the regimes representing combustion in corrugated flamelets and the thin reaction zones", *Phys. Fluids*, 19,105109 (2007).

TABLES

Quantity	Three-dimensional term	Two-dimensional term	Correction factor
Generalised FSD	$\Sigma_{gen} = \Sigma_{3D}$	Σ_{2D}	$4/\pi$
Tangential strain rate term	$\overline{(a_T)}_s \Sigma_{gen}$	$\overline{(a_T)}_{s2} \Sigma_{2D}$	$8/\pi$
Surface averaged displacement speed	$\overline{(S_d)}_s$	$\overline{(S_{d2D})}_{s2}$	$\pi/4$
Propagation term	$-\frac{\partial \overline{(S_d N_i)}_s \Sigma_{gen}}{\partial x_i}$	$-\frac{\partial \overline{(S_{d2D})}_{s2} \overline{(M_i)}_{s2} \Sigma_{gen}}{\partial x_i}$	$\pi/4$
Surface averaged curvature	$\overline{(\kappa_m)}_s$	$\overline{(k_2)}_{s2}$	$\pi/2$
Curvature term	$2\overline{(S_d \kappa_m)}_s \Sigma_{gen}$	$2\overline{(S_{d2D} k_2)}_{s2} \Sigma_{2D}$	$4/\pi$

Table I: The list of correction factors relating two-dimensional and three-dimensional FSD related quantities according to theoretical analysis.

Case (Grid size)	**Regime of combustion**	u'/S_L	l/δ_{th}	τ	*Le*	Re_t	*Da*	*Ka*
A $(261\times128\times128)$	Corrugated flamelets	1.41	9.64	2.3	1.00	56.70	6.84	0.54
B $(230\times230\times230)$	Thin reaction zones	7.50	2.45	3.0	1.00	46.86	0.330	13.12
C $(230\times230\times230)$	Thin reaction zones	7.50	2.45	4.5	0.34	46.86	0.330	13.12
D $(230\times230\times230)$	Thin reaction zones	7.50	2.45	4.5	0.60	46.86	0.330	13.12
E $(230\times230\times230)$	Thin reaction zones	7.50	2.45	4.5	0.80	46.86	0.330	13.12
F $(230\times230\times230)$	Thin reaction zones	7.50	2.45	4.5	1.00	46.86	0.330	13.12
G $(230\times230\times230)$	Thin reaction zones	7.50	2.45	4.5	1.20	46.86	0.330	13.12
H $(345\times230\times230)$	Thin reaction zones	5.00	1.67	4.5	1.00	22.00	0.334	8.67
I $(345\times230\times230)$	Thin reaction zones	6.25	1.44	4.5	1.00	23.50	0.230	13.00
J $(345\times230\times230)$	Thin reaction zones	7.50	2.50	4.5	1.00	47.85	0.334	13.00
K $(345\times230\times230)$	Thin reaction zones	9.00	4.31	4.5	1.00	100.00	0.480	13.00
L $(345\times230\times230)$	Thin reaction zones	11.25	3.75	4.5	1.00	110.00	0.334	19.50

Table II: Simulation parameters corresponding to the DNS database.

Corr. / c	$S_d - \kappa_m$	$\Sigma_3 - \kappa_m$
$c = 0.1$	-0.876 (A);-0.883 (B) -0.790 (C);-0.817 (D) -0.870 (E);-0.880 (F) -0.889 (G);-0.910 (H) -0.913 (I);-0.882 (J) -0.815 (K);-0.843 (L)	0.765 (A);-0.115 (B) 0.396 (C);0.170 (D) -0.022 (E);-0.148 (F) -0.195 (G);-0.118(H) -0.088 (I);-0.093 (J) -0.060 (K);-0.044 (L)
$c = 0.3$	-0.890 (A);-0.953 (B) -0.785 (C);-0.837 (D) -0.939 (E);-0.965 (F) -0.950 (G);-0.988 (H) -0.989 (I);-0.879 (J) -0.933 (K);-0.916 (L)	0.813 (A);-0.090 (B) 0.571 (C);0.458 (D) 0.199 (E);-0.131 (F) -0.338 (G);-0.074 (H) -0.021 (I);-0.031 (J) -0.140 (K);0.033 (L)
$c = 0.5$	-0.397 (A);-0.945 (B) -0.693(C);-0.832 (D) -0.937 (E);-0.948 (F) -0.921 (G);-0.974 (H) -0.975 (I);-0.943 (J) -0.844 (K);-0.904 (L)	0.400 (A);-0.077 (B) 0.598 (C);0.638 (D) 0.428 (E);-0.135 (F) -0.622 (G);-0.166 (H) -0.104 (I);0.021 (J) -0.124 (K);0.077 (L)
$c = 0.7$	-0.744 (A);-0.867 (B) -0.455 (C);-0.805 (D) -0.866 (E);-0.874 (F) -0.840 (G);-0.931 (H) -0.933 (I);-0.826 (J) -0.730 (K);-0.807 (L)	0.660 (A);-0.170 (B) 0.417 (C);0.733 (D) 0.538 (E);-0.223 (F) -0.814 (G);-0.296 (H) -0.164 (I);-0.105 (J) -0.174 (K);-0.012 (L)
$c = 0.9$	-0.302 (A);-0.675 (B) -0.268 (C);-0.613 (D) -0.709 (E);-0.714 (F) -0.694 (G);-0.840 (H) -0.848 (I);-0.727 (J) -0.490 (K);-0.566 (L)	0.878 (A);-0.331 (B) 0.698 (C);0.708 (D) 0.439 (E);-0.402 (F) -0.878 (G);-0.481 (H) -0.310 (I);-0.300 (J) -0.420 (K);-0.183 (L)

Table III: Correlation coefficients for the $S_d - \kappa_m$, $(S_r + S_n) - \kappa_m$ and $\Sigma_3 - \kappa_m$ correlations for different c isosurfaces through the flame brush.

Corr. / c	$S_{d2D} - k_2$	$\Sigma_2 - k_2$
$c = 0.1$	-0.354 (A);-0.603 (B) 0.393 (C);-0.321 (D) -0.597 (E);-0.621 (F) -0.638 (G);-0.610 (H) -0.628 (I);-0.495 (J) -0.353 (K);-0.460 (L)	0.268 (A);-0.083 (B) 0.262 (C);0.113 (D) -0.014 (E);-0.014 (F) -0.014 (G);-0.083 (H) -0.061 (I);-0.072 (J) -0.03 (K);-0.042 (L)
$c = 0.3$	-0.490 (A);-0.682 (B) 0.298 (C);-0.379 (D) -0.657 (E);-0.673 (F) -0.687 (G);-0.690 (H) -0.700 (I);-0.467 (J) -0.503 (K);-0.564 (L)	0.389 (A);-0.068 (B) 0.350 (C);0.283 (D) -0.021 (E);-0.021 (F) -0.021 (G);-0.024 (H) 0.033 (I);0.006 (J) -0.076(K);0.023 (L)
$c = 0.5$	-0.042 (A);-0.652 (B) 0.233 (C);-0.391 (D) -0.660 (E);-0.680 (F) -0.696 (G);-0.704 (H) -0.700 (I);-0.534 (J) -0.450 (K);-0.565 (L)	-0.189 (A);-0.032 (B) 0.388 (C);0.376 (D) -0.031 (E);-0.031 (F) -0.03 (G);-0.038 (H) -0.028 (I);-0.004 (J) -0.064 (K); 0.034 (L)
$c = 0.7$	-0.186 (A);-0.626 (B) 0.055 (C);-0.417 (D) -0.649 (E);-0.656 (F) -0.659 (G);-0.678 (H) -0.675 (I);-0.514 (J) -0.431 (K);-0.521 (L)	-0.033 (A);-0.051 (B) 0.354 (C);0.420 (D) -0.034 (E);-0.034 (F) -0.034 (G);-0.044 (H) -0.045 (I);-0.052 (J) -0.071 (K);-0.010 (L)
$c = 0.9$	-0.278 (A);-0.506 (B) -0.048 (C);-0.352 (D) -0.585 (E);-0.570 (F) -0.561 (G);-0.625 (H) -0.614 (I);-0.517(J) -0.333 (K);-0.389 (L)	0.464 (A);-0.087 (B) 0.420 (C);0.386 (D) -0.029 (E);-0.029 (F) -0.029 (G);-0.055 (H) -0.071 (I);-0.088 (J) -0.140 (K);-0.070 (L)

Table IV: Correlation coefficients for the $S_{d2D} - k_2$ and $\Sigma_2 - k_2$ correlations for different c isosurfaces through the flame brush.

FIGURE CAPTIONS

Fig. 1: Coordinates and reference frames used in the analysis.

Fig. 2: Variations of $\Sigma_{gen} \times \delta_{th}$, $\Sigma_{2D} \times \delta_{th}$ and $(4/\pi) \times \Sigma_{2D} \times \delta_{th}$ with $\tilde{c}$ across the flame brush for cases: (a) A, (b) B, (c) C, (d) E, (e) F, (f) G.

Fig. 3: Variations of $\Sigma_{gen} \times \delta_{th}$, $\Sigma_{2D} \times \delta_{th}$ and $(4/\pi) \times \Sigma_{2D} \times \delta_{th}$ with $\tilde{c}$ across the flame brush for cases: (a) H, (b) J, (c) L.

Fig. 4: Variations of $\overline{(a_T)}_s \Sigma_{gen} \times \delta_{th}^2 / S_L$, $\overline{(a_{T2D})}_{s2} \Sigma_{2D} \times \delta_{th}^2 / S_L$ and $8/\pi \times \overline{(a_{T2D})}_{s2} \Sigma_{2D} \times \delta_{th}^2 / S_L$ with $\tilde{c}$ across the flame brush for cases: (a) A, (b) B, (c) C, (d) E, (e) F, (f) G.

Fig. 5: Variations of $\overline{(a_T)}_s \Sigma_{gen} \times \delta_{th}^2 / S_L$, $\overline{(a_{T2D})}_{s2} \Sigma_{2D} \times \delta_{th}^2 / S_L$ and $8/\pi \times \overline{(a_{T2D})}_{s2} \Sigma_{2D} \times \delta_{th}^2 / S_L$ with $\tilde{c}$ across the flame brush for cases : (a) H, (b) J, (c) L.

Fig. 6: Variations of $\overline{(S_d N_1)}_s \Sigma_{gen} \times \delta_{th} / S_L$, $\overline{(S_{d2D})}_{s2} \overline{(M_1)}_{s2} \Sigma_{2D} \times \delta_{th} / S_L$ and $\pi/4 \times \overline{(S_{d2D})}_{s2} \overline{(M_1)}_{s2} \Sigma_{2D} \times \delta_{th} / S_L$ with $\tilde{c}$ across the flame brush for cases: (a) A, (b) B, (c) C, (d) E, (e) G, (f) I, (g) J, (h) K.

Fig. 7: Variations of $\overline{(\kappa_m)}_s \times \delta_{th}$, $\overline{(k_2)}_{s2} \times \delta_{th}$ and $\pi/2 \times \overline{(k_2)}_{s2} \times \delta_{th}$ with $\tilde{c}$ across the flame brush for cases: (a) A, (b) B, (c) C, (d) E, (e) G, (f) I, (g) J, (h) K.

Fig. 8: Variations of $2\overline{(S_d \kappa_m)}_s \Sigma_{gen} \times \delta_{th}^2 / S_L$, $2\overline{(S_{d2D} k_2)}_{s2} \Sigma_{2D} \times \delta_{th}^2 / S_L$ and $(4/\pi) \times 2\overline{(S_{d2D} k_2)}_{s2} \Sigma_{2D} \times \delta_{th}^2 / S_L$ with $\tilde{c}$ across the flame brush for cases: (a) A, (b) B, (c) C, (d) E, (e) F, (f) G.

Fig. 9: Variations of $2\overline{(S_d \kappa_m)}_s \Sigma_{gen} \times \delta_{th}^2 / S_L$, $2\overline{(S_{d2D} k_2)}_{s2} \Sigma_{2D} \times \delta_{th}^2 / S_L$ and $(4/\pi) \times 2\overline{(S_{d2D} k_2)}_{s2} \Sigma_{2D} \times \delta_{th}^2 / S_L$ with $\tilde{c}$ across the flame brush for cases: (a) H, (b) J, (c) L.

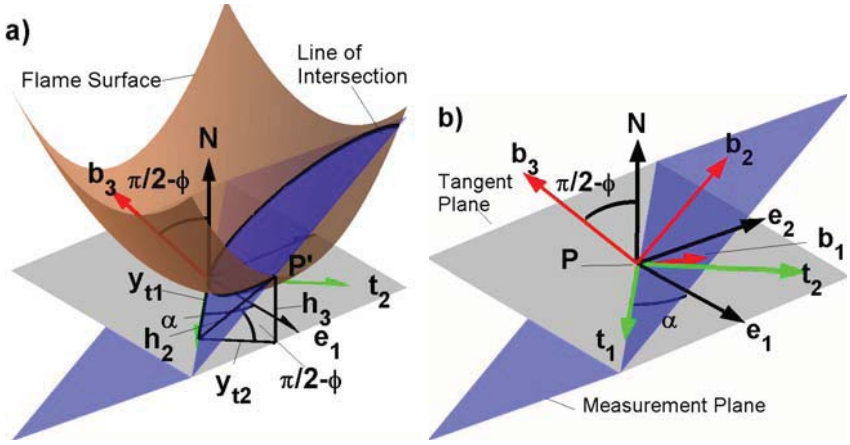

Fig. 1: Coordinates and reference frames used in the analysis.

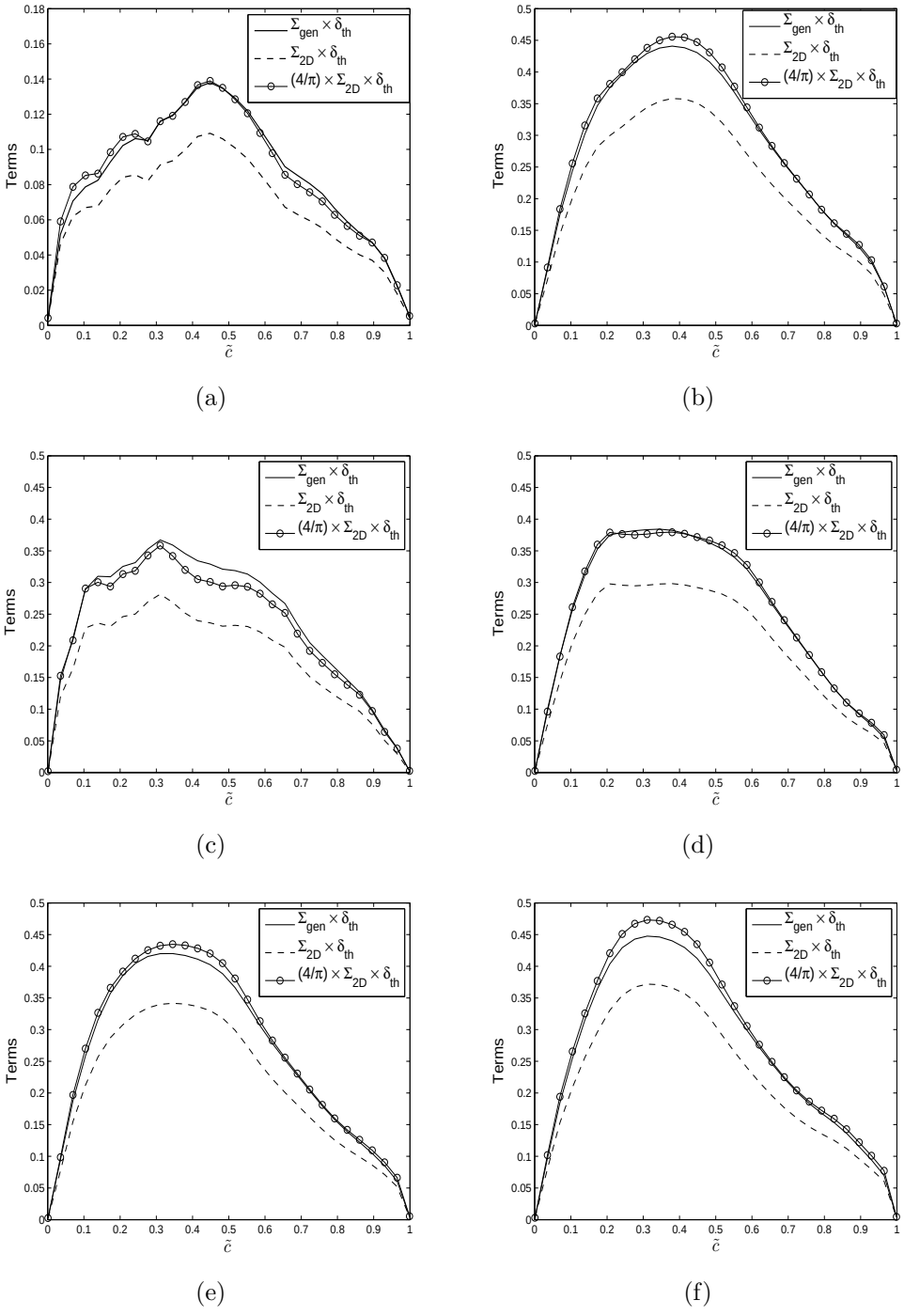

Figure 2: Variations of $\Sigma_{gen} \times \delta_{th}$, $\Sigma_{2D} \times \delta_{th}$ and $(4/\pi) \times \Sigma_{2D} \times \delta_{th}$ with across the flame brush for cases: (a) A, (b) B, (c) C, (d) E, (e) F, (f) G.

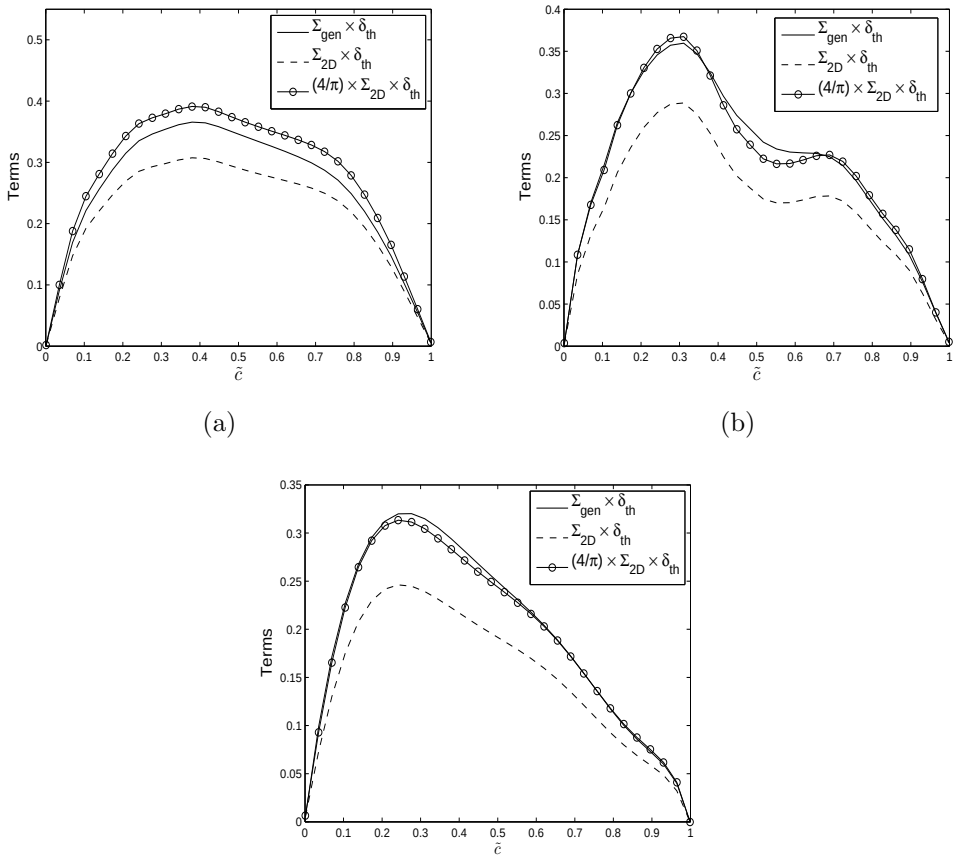

Figure 3: Variations of $\Sigma_{gen} \times \delta_{th}$, $\Sigma_{2D} \times \delta_{th}$ and $(4/\pi) \times \Sigma_{2D} \times \delta_{th}$ with $\tilde{c}$ across the flame brush for cases: (a) H, (b) J, (c) L.

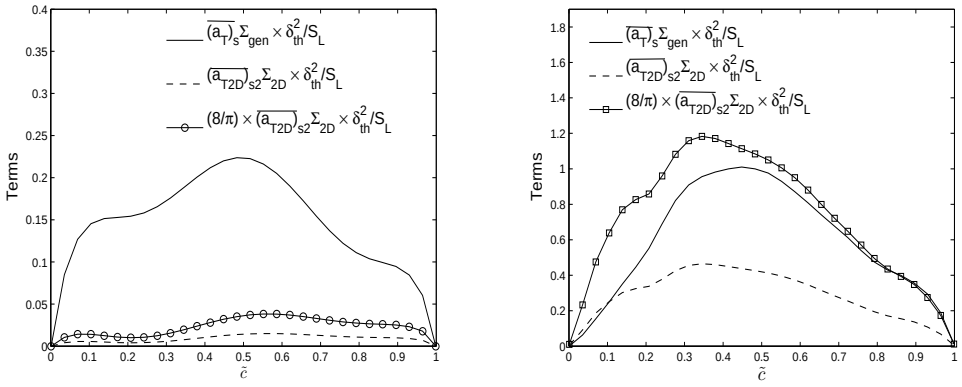

(a) (b)

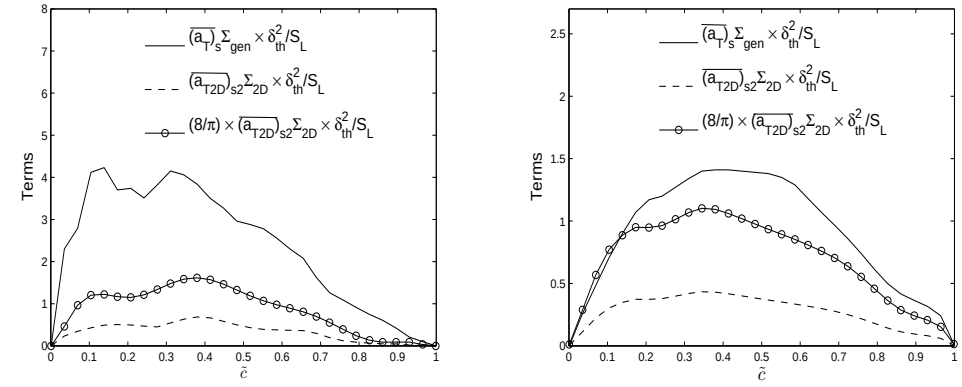

(c) (d)

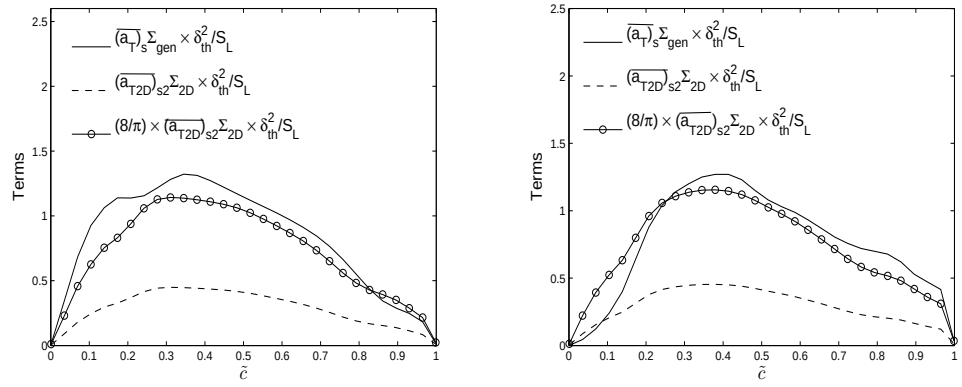

(e) (f)

Figure 4: Variations of $\overline{(a_T)}_s\Sigma_{gen}\times\delta_{th}^2/S_L$, $\overline{(a_{T2D})}_{s2D}\Sigma_{2D}\times\delta_{th}^2/S_L$ and $8/\pi\times\overline{(a_{T2D})}_{s2D}\Sigma_{2D}\times\delta_{th}^2/S_L$ with $\tilde{c}$ across the flame brush for cases: (a) A, (b) B, (c) C, (d) E, (e) F, (f) G.

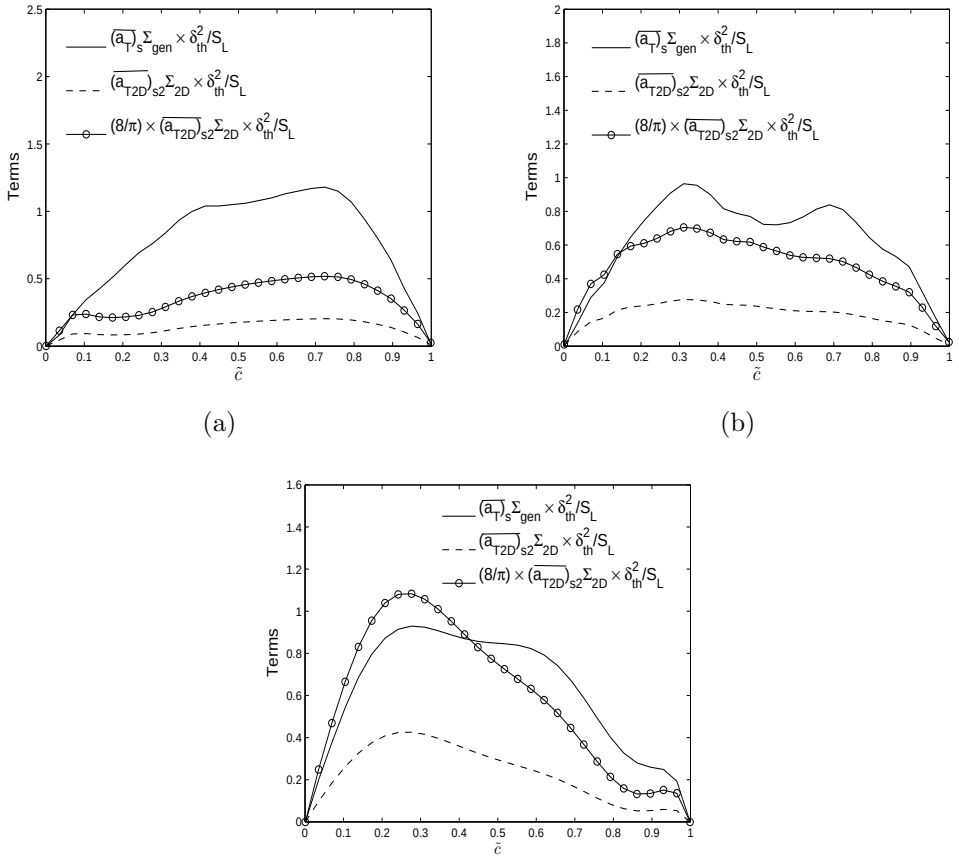

(a) (b)

(c)

Figure 5: Variations of $\overline{(a_T)}_s\Sigma_{gen}\times\delta_{th}^2/S_L$, $\overline{(a_{T2D})}_{s2D}\Sigma_{2D}\times\delta_{th}^2/S_L$ and $8/\pi\times\overline{(a_{T2D})}_{s2D}\Sigma_{2D}\times\delta_{th}^2/S_L$ with $\tilde{c}$ across the flame brush for cases : (a) H, (b) J, (c) L.

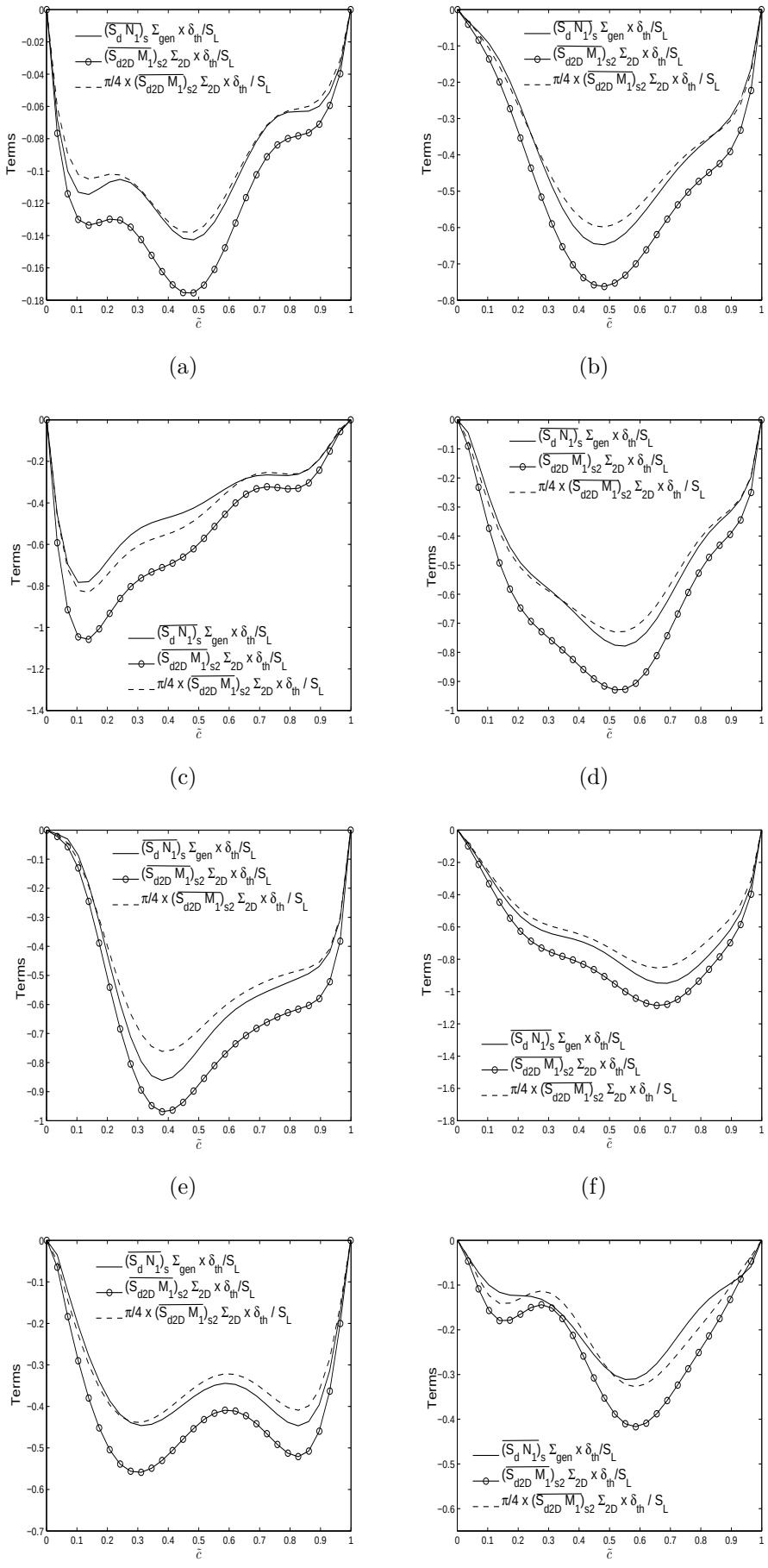

Figure 6: Variations of $\overline{(S_d N_1)}_s \Sigma_{gen} \times \delta_{th}/S_L$, $\overline{(S_{d2D})}_{s2} \overline{(M_1)}_{s2} \Sigma_{2D} \times \delta_{th}/S_L$ and $\pi/4 \times \overline{(S_{d2D})}_{s2} \overline{(M_1)}_{s2} \Sigma_{2D} \times \delta_{th}/S_L$ with $\tilde{c}$ across the flame brush for cases: (a) A, (b) B, (c) C, (d) E, (e) G, (f) I, (g) J, (h) K.

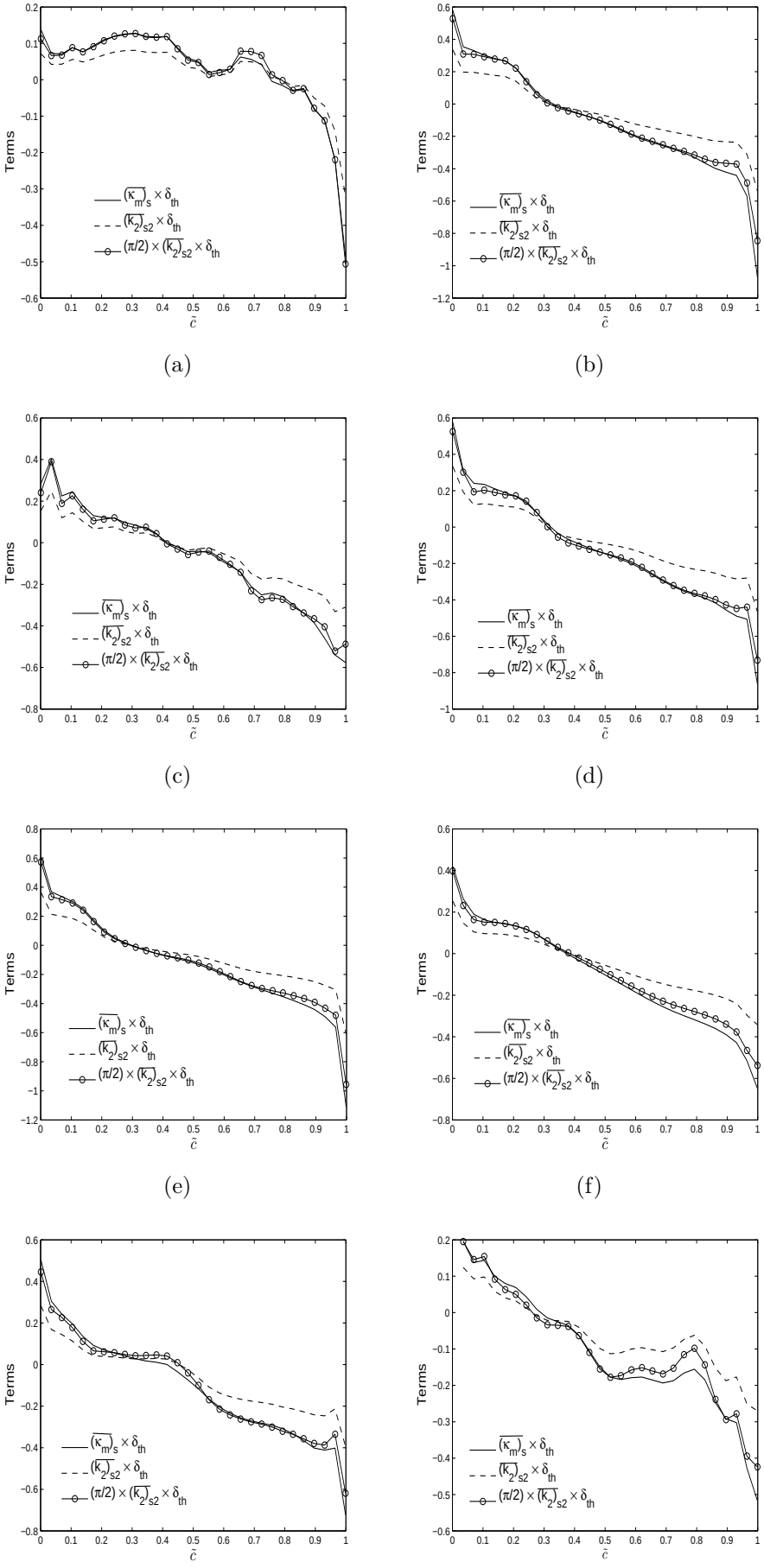

Figure 7: Variations of $\overline{(\kappa_m)}_s \times \delta_{th}$, $\overline{(k_2)}_{s2} \times \delta_{th}$ and $\pi/2 \times \overline{(k_2)}_{s2} \times \delta_{th}$ with across the flame brush for cases: (a) A, (b) B, (c) C, (d) E, (e) G, (f) I, (g) J, (h) K.

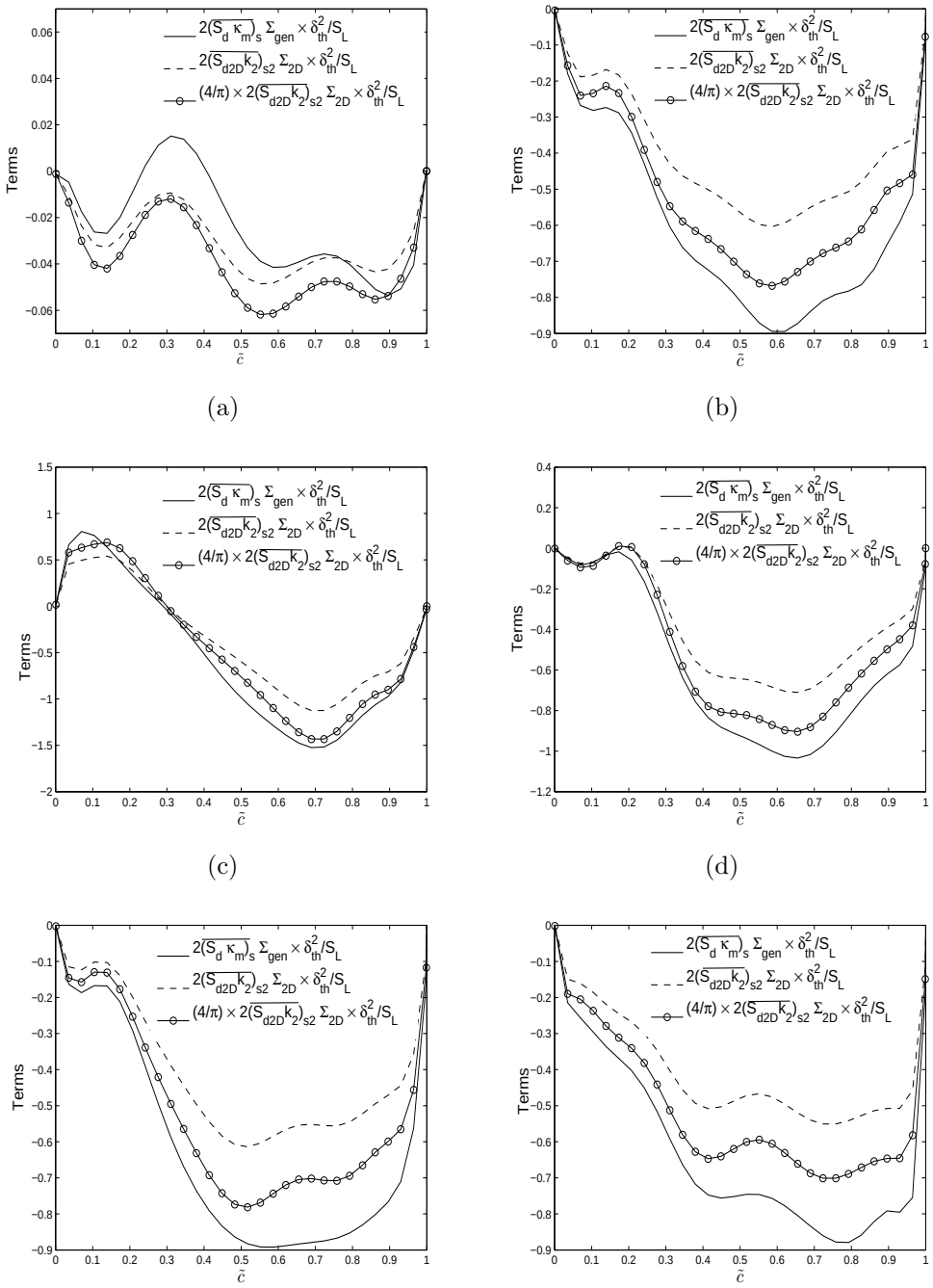

Figure 8: Variations of $2\overline{(S_d\kappa_m)}_s\Sigma_{gen} \times \delta_{th}^2/S_L$, $2\overline{(S_{d2D}k_2)}_{s2}\Sigma_{2D} \times \delta_{th}^2/S_L$ and $(4/\pi) \times 2\overline{(S_{d2D}k_2)}_{s2}\Sigma_{2D} \times \delta_{th}^2/S_L$ with $\tilde{c}$ across the flame brush for cases: (a) A, (b) B, (c) C, (d) E, (e) F, (f) G.

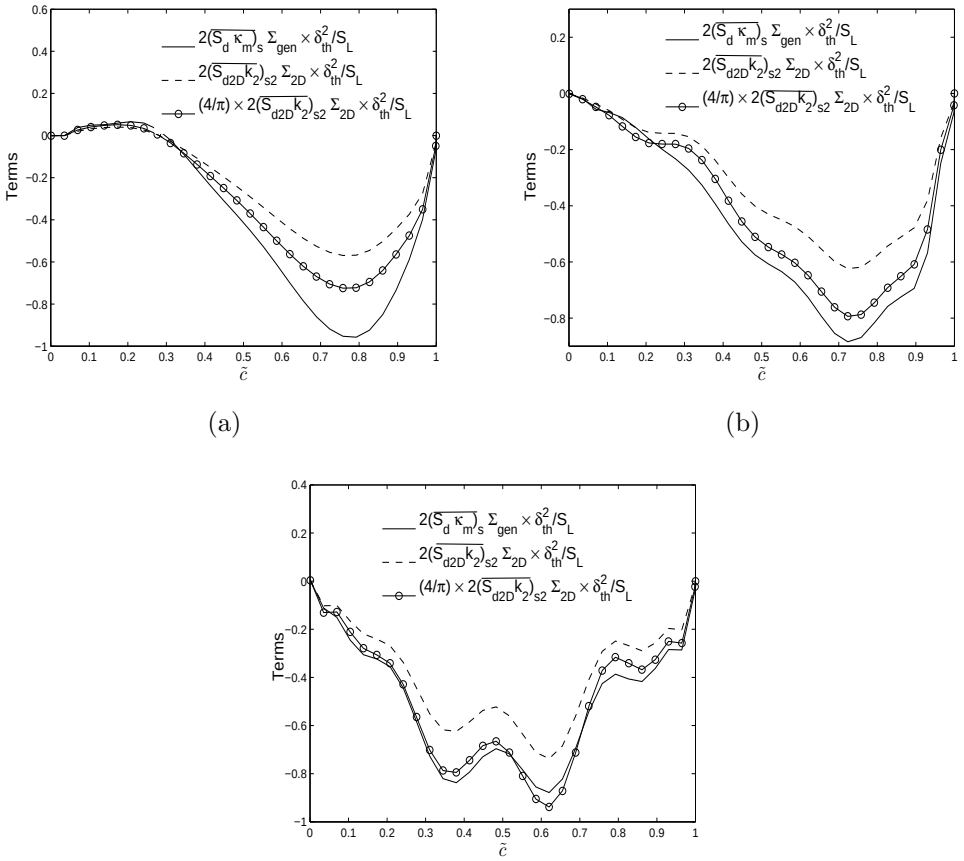

(a) (b)

(c)

Figure 9: Variations of $2\overline{(S_d\kappa_m)}_s\Sigma_{gen} \times \delta_{th}^2/S_L$, $2\overline{(S_{d2D}k_2)}_{s2}\Sigma_{2D} \times \delta_{th}^2/S_L$ and $(4/\pi) \times 2\overline{(S_{d2D}k_2)}_{s2}\Sigma_{2D} \times \delta_{th}^2/S_L$ with $\tilde{c}$ across the flame brush for cases: (a) H, (b) J, (c) L.